



Bifunctional glycosphingolipid (GSL) probes to investigate GSL-interacting proteins in cell membranes

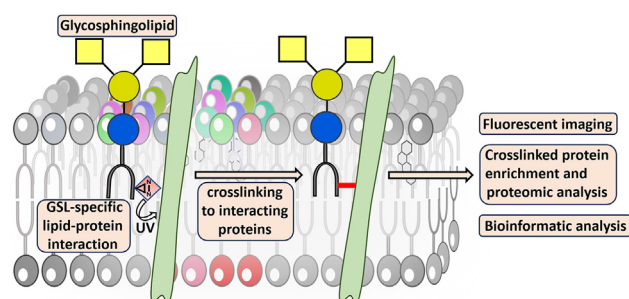
Sayan Kundu^{1,*}, Rajendra Rohokale^{1,*}, Chuwei Lin², Sixue Chen^{2,3}, Shayak Biswas¹, and Zhongwu Guo^{1,*}

¹Department of Chemistry, and ²Department of Biology, Genetics Institute, University of Florida, Gainesville, FL, USA; ³Department of Biology, University of Mississippi, Oxford, MS, USA

Abstract Glycosphingolipids (GSLs) are abundant glycolipids on cells and essential for cell recognition, adhesion, signal transduction, and so on. However, their lipid anchors are not long enough to cross the membrane bilayer. To transduce transmembrane signals, GSLs must interact with other membrane components, whereas such interactions are difficult to investigate. To overcome this difficulty, bifunctional derivatives of $\text{II}^3\text{-}\beta\text{-N-acetyl-D-galactosamine-GA2}$ (GalNAc-GA2) and $\beta\text{-N-acetyl-D-glucosamine-ceramide}$ (GlcNAc-Cer) were synthesized as probes to explore GSL-interacting membrane proteins in live cells. Both probes contain photoreactive diazirine in the lipid moiety, which can crosslink with proximal membrane proteins upon photoactivation, and clickable alkyne in the glycan to facilitate affinity tag addition for crosslinked protein pull-down and characterization. The synthesis is highlighted by the efficient assembly of simple glycolipid precursors followed by on-site lipid remodeling. These probes were employed to profile GSL-interacting membrane proteins in HEK293 cells. The GalNAc-GA2 probe revealed 312 distinct proteins, with GlcNAc-Cer probe-crosslinked proteins as controls, suggesting the potential influence of the glycan on GSL functions. Many of the proteins identified with the GalNAc-GA2 probe are associated with GSLs, and some have been validated as being specific to this probe. The versatile probe design and experimental protocols are anticipated to be widely applicable to GSL research.

Supplementary key words glycolipids • glycosphingolipids • ceramides • chemical synthesis • proteomics • fluorescence microscopy • protein-lipid interaction • diazirine • photoactivated crosslinking • click reaction

Glycosphingolipids (GSLs) are glycolipids consisting of a hydrophilic glycan as the head group and a hydrophobic ceramide (Cer) as the backbone, which are stitched together by a glycosidic bond (Fig. 1) (1). Their distinctive structures and biophysical properties, for



example, being able to form specific microdomains in the cell membrane (2–5), warrant GSLs a unique niche in cell biology. For example, GSLs are a principal and essential membrane constituent (6–8) functioning as receptors on the cell surface (9, 10); thus, many exoplasmic and cell surface proteins contain GSL-binding domains (11–13). As such, GSLs are involved in regulating various physiological and pathological events like signal transduction (14), cell differentiation and proliferation (15–17), cancer (18), Alzheimer's disease (19–21), and microbial infection (22–24). LcGg4 in Fig. 1 is an illustrative example of GSLs, representing the LcGg series core structure (25), and a leukemia-associated GSL antigen as well (26). It has been further demonstrated that the interactions between GSLs and their ligands are regulated by both their glycan moiety and their lipid anchor (9, 27).

Despite the documented involvement of GSLs in various cellular activities, the exact mechanisms by which GSLs transduce binding signals through the cell membrane remain ambiguous. In general, it is believed that GSLs can generate specific microdomains in the membrane, such as the “lipid rafts,” which serve as platforms to recruit other biomolecules to facilitate their interactions with GSLs (28–31). Although extracellular ligands can directly bind GSLs (31, 32), the lipid

*These authors contributed equally to the current work.

*For correspondence: Zhongwu Guo, zguo@chem.ufl.edu.

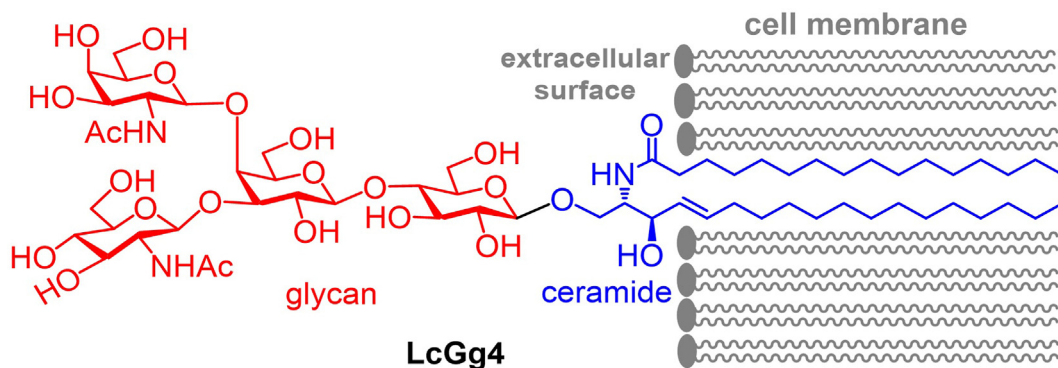


Fig. 1. The chemical structure of LcGg4, a representative GSL and a cancer antigen, and its association with the cell membrane.

chains of GSLs are usually not long enough to cross the entire membrane bilayer. To transduce signals induced by GSL binding with extracellular ligands across the cell membrane, GSLs must communicate with other cell membrane components. Unfortunately, cell membrane components interacting with GSLs are difficult to identify due to the highly diverse, complex, and dynamic structures and nature of GSLs and the cell membrane.

To investigate lipid–protein interactions, several proteome-wide mapping methods have been explored, which include microarrays of various metabolites to profile lipid-binding proteins (33), proteome chip-based screening (34), affinity-based protein purification by columns or lipid immobilized magnetic beads (35, 36), and so on. Various model membranes (e.g., nanodiscs, liposomes, and supported bilayers) have also been employed to examine the interactions of GSLs with proteins by mass spectrometry (MS) and competitive ligand binding assays (37, 38). As a result, many proteins, such as Galectin (39), death receptor Fas (40), notch ligand delta-like 1 protein (41), Serotonin (42), insulin receptors (43), and numerous growth factor receptors (44–52), have been found to interact with GSLs. However, a main limitation of these methods is that the lipids or proteins immobilized onto solid supports are not in their natural state. Moreover, the most important mechanism of lipid–protein interactions, that is, hydrophobic matching between the lipid tails of GSLs and the hydrophobic domains of proteins is likely to be neglected. To address these problems, specially functionalized probes have drawn significant attention in recent years. Typically, such probes contain two functional groups, one crosslinking with target molecules and the other enabling the isolation and characterization of cross-linked molecules (53–58). A trifunctional probe containing photocage, photoreactive diazirine, and clickable alkyne moieties was also developed to explore the signaling events of sphingosine and diacylglycerol (59).

The present research aimed to develop a practicable approach for the identification of membrane proteins interacting with GSLs. To this end, we have designed and synthesized two bifunctional GSL analogs that contain photoreactive diazirine to facilitate GSL crosslinking with interacting proteins and clickable alkyne to enable the introduction of an affinity tag for crosslinked protein isolation. These GSL analogs were used as demonstrating probes to explore GSL-interacting proteins in the membrane of HEK293 cells.

MATERIALS AND METHODS

General methods and materials

Chemicals and materials were purchased from commercial sources and used as received without further purification unless noted otherwise. Molecular sieves 4 Å (MS 4 Å) were flame-dried under a high vacuum and used immediately after being cooled to rt in an N₂ atmosphere. Analytical thin layer chromatography (TLC) was carried out on silica gel 60 Å F254 plates with detection by a UV detector and/or by charring with 10% (v/v) H₂SO₄ in ethanol. Flash column chromatography was performed on silica gel 60 (230–400 Mesh). NMR spectra were acquired on a 400 or 600 MHz NMR spectrometer with chemical shifts reported in ppm (δ) referenced to CDCl₃ (residual ¹H NMR: δ 7.26 ppm, ¹³C NMR: δ 77.16 ppm) or CD₃OD (residual ¹H NMR: δ 3.31 ppm, ¹³C NMR: δ 49.0 ppm). Peak and coupling constant assignments are made based on ¹H, ¹H–¹H COSY, ¹H–¹³C HSQC, and ¹H–¹³C HMBC experiments, and structural elucidations were made with additional information from gCOSY, gHSQC, and gHMBC experiments. Aluminum heating blocks were used for heating. Paraformaldehyde (PFA), copper sulfate (CuSO₄), sodium ascorbate, poly-L-lysine, and tris(2-carboxyethyl) phosphine hydrochloride (TCEP) were from Sigma Aldrich. Fetal bovine serum (FBS), Dulbecco's Modified Eagle's Medium (DMEM), and penicillin-streptomycin solution were from the American Type Culture Collection (ATCC). Dulbecco's phosphate buffer saline (DPBS), 4',6-diamidino-2-phenylindole (DAPI), streptavidin Agarose resin, Cy5-azide, bovine serum albumin (BSA), Pierce™ anti-DYKDDDDK magnetic agarose beads, and lipofectamine™

2000 transfection reagent were from Thermo Fisher scientific. Biotin-azide (or Biotin-PEG3-Azide) and tris-(3-hydroxypropyl)triazolymethylamine (THPTA) were from Click Chemistry Tools. Streptavidin-A488 was from Santa Cruz Biotech. RPMI 1640 buffer was from Lonza. Fluorescent imaging was performed on an Olympus IX71 inverted system equipped with LED light source (Cool LED, PE-300), 20X 0.8 and 60X 1.25 NA plan apochromatic objectives (Olympus LUCPlanFI N objective), DAPI and Cy5 fluorescence channels, and Olympus DP23M color camera. Image analysis was performed using Olympus Cellsens Standard 3 and FIJI/ImageJ software. The cell lysis buffer contained 4% sodium dodecyl sulfate (SDS), 120 mM NaCl, and 50 mM triethanolamine. The cell permeabilization buffer is 1× DPBS with 0.1% Triton-X-100% and 2.5% BSA. For VPS36, SNX5, and RAB27A protein overexpression, VPS36, SNX5, and RAB27A cDNA ORF Clones, Human, Flag tag plasmids were purchased from Sino Biological. Organelle markers utilized in this work are listed in the [Supplemental data](#) with corresponding catalog numbers.

(2S,3R)-2-(tert-Butyloxycarbonyl)amino-3-pivaloyloxypent-4-en-1-yl 3,4,6-tri-O-acetyl-2-deoxy-2-(2,2,2-trichloroethoxycarbonylamino)-β-D-glucopyranoside (6)

A mixture of **4** (0.61 g, 0.98 mmol), **5** (0.27 g, 0.89 mmol), and flame-dried MS 4Å (1.0 g) in dry dichloromethane (DCM, 10 ml) was stirred at room temperature (rt) under Argon for 30 min before cooling to -78°C . Trimethylsilyl triflate (TMSOTf, 8.2 μl , 0.05 mmol) was added, and the mixture was allowed to warm to -30°C and kept at this temperature for 1 h. TLC analysis confirmed the complete consumption of starting materials, and trimethylamine was added to quench the reaction. The mixture was filtered through a Celite pad, and the filtrate was concentrated in a vacuum. The product was purified by flash chromatography (Hexane/EtOAc 1/1) to afford **6** as a colorless syrup (0.60 g, 88%). TLC: $R_f = 0.46$ (Hexane/EtOAc 1:1). ^1H NMR (600 MHz, CDCl_3): δ 5.77 (ddd, $J = 17.1, 10.6, 6.1$ Hz, 1H, =CH), 5.40–5.26 (m, 3H, -C=CH₂), 5.24–5.22 (m, 2H), 5.04 (t, $J = 9.7$ Hz, 1H, H3), 4.85 (d, $J = 7.7$ Hz, 1H), 4.81 (d, $J = 12.0$ Hz, 1H, O-CH-Cl₃), 4.61 (d, $J = 3.6$ Hz, 1H), 4.59 (d, $J = 7.8$ Hz, 1H, anomeric H), 4.21 (dd, $J = 12.3, 4.8$ Hz, 1H), 4.16–4.07 (m, 1H), 4.06–3.99 (m, 1H), 3.95 (dd, $J = 9.9, 4.2$ Hz, 1H), 3.72–3.60 (m, 2H), 3.56 (dd, $J = 9.6, 3.7$ Hz, 1H), 2.06 (s, 3H), 2.01 (s, 3H), 2.01 (s, 3H), 1.41 (s, 9H), 1.18 (s, 9H). ^{13}C NMR (151 MHz, CDCl_3): δ 177.0, 170.9, 170.7, 169.5, 155.5, 154.2, 133.2, 118.7, 100.8, 100.7, 95.5, 79.8, 74.6, 73.3, 73.3, 71.9, 71.9, 68.6, 68.0, 62.1, 60.5, 56.2, 52.0, 38.9, 28.5, 27.1, 20.8, 20.7, 20.7. HRMS (ESI-TOF) m/z : [M + H]⁺ Calcd for C₃₀H₄₆Cl₃N₂O₁₄ 763.2009; Found 763.2022.

(2S,3R,E)-2-(tert-Butyloxycarbonyl)amino-3-pivaloyloxyoctadec-4-en-1-yl 3,4,6-tri-O-acetyl-2-deoxy-2-(2,2,2-trichloroethoxycarbonylamino)-β-D-glucopyranoside (8)

To a solution of **6** (201 mg, 0.26 mmol) and pentadec-1-ene **7** (0.43 ml, 1.58 mmol) in dry DCM (65 ml) was added second-generation Hoveyda–Grubbs catalyst (16.5 mg, 0.026 mmol). The mixture was refluxed for 5 days, while a batch of **7** (0.43 ml, 1.58 mmol) and Hoveyda–Grubbs catalyst (5 mol%) was added at 24-h intervals. After the reaction was complete, 2 drops of dimethyl sulfoxide (DMSO) were added at rt, followed by stirring for another 2 h. The mixture was concentrated, and the product was purified by silica gel column

chromatography to give **8** (206 mg, 83%) as a white solid. TLC: $R_f = 0.7$ (Hexane/EtOAc 2:3). ^1H NMR (600 MHz, CDCl_3): δ 5.77 (dt, $J = 14.1, 6.7$ Hz, 1H, C=CH-CH₂), 5.35 (dd, $J = 15.3, 7.4$ Hz, 1H, -C=CH-C), 5.28–5.18 (m, 3H), 5.06 (t, $J = 9.6$ Hz, 1H), 4.94–4.71 (m, 2H), 4.64–4.64 (m, 2H), 4.22 (dd, $J = 12.3, 4.7$ Hz, 1H), 4.10 (dd, $J = 12.3, 2.2$ Hz, 1H), 4.01–3.95 (m, 1H), 3.93 (dd, $J = 9.9, 4.3$ Hz, 1H), 3.72–3.65 (m, 1H), 3.62 (q, $J = 8.8$ Hz, 1H), 3.59–3.53 (m, 1H), 2.07 (s, 3H), 2.03 (s, 3H), 2.02 (s, 3H), 2.01–1.96 (m, 2H), 1.42 (s, 9H), 1.38–1.22 (m, 22H), 1.17 (s, 9H), 0.87 (t, $J = 7.0$ Hz, 3H). ^{13}C NMR (151 MHz, CDCl_3): δ 176.9, 170.7, 169.5, 155.5, 154.2, 137.1, 124.6, 100.6, 95.5, 79.8, 74.6, 73.3, 72.0, 71.9, 68.6, 68.1, 62.1, 56.3, 52.2, 38.9, 32.4, 32.0, 29.8, 29.7, 29.7, 29.6, 29.4, 29.3, 29.0, 28.5, 27.1, 22.8, 20.8, 20.7. HRMS (ESI-TOF) m/z : [M + H]⁺ Calcd for C₄₃H₇₂Cl₃N₂O₁₄ 945.4062; Found 945.4044.

(2S,3R,E)-2-(tert-Butyloxycarbonyl)amino-3-pivaloyloxyoctadec-4-en-1-yl 3,4,6-tri-O-acetyl-2-deoxy-2-(pent-4-ynamido)-β-D-glucopyranoside (9)

To a solution of **8** (39 mg, 0.041 mmol) in acetic acid (AcOH)/tetrahydrofuran (1:3, 2 ml) was added activated Zn (134.5 mg, 2.06 mmol). After the mixture was stirred at rt for 12 h, it was filtered through a Celite pad, and the filtrate was concentrated in vacuo. The product was washed with dry toluene (3 × 3 ml) and then dissolved in 1 ml of dry DCM. To this solution were added pent-4-ynic acid (20.1 mg, 0.204 mmol), 1-ethyl-3-(3-dimethylaminopropyl)carbodiimide (EDC, 39.2 mg, 0.204 mmol), and 4-dimethylaminopyridine (DMAP, 5 mg, 0.041 mmol) in 2 ml of dry DCM at 0°C. The mixture was stirred at rt overnight and diluted with DCM. The organic layer was washed with saturated NaHCO₃, water, and brine, and dried over Na₂SO₄. The solution was concentrated under vacuum and the residue was separated by silica gel column chromatography to give **9** (24.8 mg, 71%) as colorless syrup. TLC: $R_f = 0.74$ (EtOAc/Hexane 4:1). ^1H NMR (600 MHz, CDCl_3): δ 5.88–5.70 (m, 2H), 5.35 (dd, $J = 15.3, 7.4$ Hz, 1H), 5.31–5.25 (m, 1H), 5.20 (t, $J = 7.1$ Hz, 1H), 5.05 (t, $J = 9.6$ Hz, 1H), 4.87 (d, $J = 9.5$ Hz, 1H, -CONH), 4.65 (d, $J = 8.2$ Hz, 1H, anomeric), 4.22 (dd, $J = 12.3, 4.8$ Hz, 1H), 4.10 (dd, $J = 12.2, 2.2$ Hz, 1H), 4.01–3.93 (m, 1H), 3.91 (dd, $J = 9.9, 4.5$ Hz, 1H), 3.83 (q, $J = 8.5$ Hz, 1H), 3.74–3.64 (m, 1H), 3.54 (dd, $J = 9.8, 3.4$ Hz, 1H), 2.53–2.46 (m, 2H), 2.42–2.33 (m, 2H), 2.07 (s, 3H), 2.03 (s, 4H, 3H × CH₃ and 1H acetylene), 2.01 (s, 3H), 2.01–1.95 (m, 2H), 1.42 (s, 9H), 1.36–1.31 (m, 2H), 1.31–1.20 (m, 20H), 1.17 (s, 9H), 0.87 (t, $J = 7.0$ Hz, 3H). ^{13}C NMR (151 MHz, CDCl_3): δ 176.9, 171.3, 170.9, 170.6, 169.4, 155.4, 136.9, 124.5, 100.6, 82.8, 82.8, 79.5, 73.3, 72.0, 71.9, 69.5, 68.5, 67.7, 62.1, 54.7, 52.2, 38.7, 35.4, 32.3, 31.9, 29.6, 29.6, 29.4, 29.3, 29.19, 28.9, 28.4, 27.0, 22.6, 20.7, 20.7, 20.6, 14.7, 14.1. HRMS (ESI-TOF) m/z : [M + H]⁺ Calcd for C₄₅H₇₅Cl₃N₂O₁₂ 851.5264; Found 851.5281.

(2S,3R,E)-2-[11-(3-Hexyl-3H-diazirin-3-yl)undecanamido]-3-(pivaloyloxy)-octadec-4-en-1-yl 3,4,6-tri-O-acetyl-2-deoxy-2-(pent-4-ynamido)-β-D-glucopyranoside (11)

Trifluoroacetic acid (TFA, 107 μl , 1.4 mmol) was added to a stirred solution of **9** (17 mg, 0.02 mmol) in DCM (3 ml) at rt, and the mixture was stirred until the disappearance of **9**. The solvent was removed in vacuo, and the residue was dissolved in dry DCM (3 ml), followed by adding EDC (7.54 mg, 0.039 mmol), DMAP (1.4 mg, 0.011 mmol), and **10** (12.2 mg, 0.039 mmol) at 0°C. The mixture was stirred under Argon at rt for 12 h. After the completion of the reaction, water was added. The organic layer was separated and washed with

saturated NaHCO₃, water, and brine and dried over Na₂SO₄. The solvent was removed in vacuo, and the residue was purified by silica gel column chromatography to afford **11** (18.4 mg, 90%) as colorless syrup. TLC: R_f = 0.8 (EtOAc/Hexane, 4:1). ¹H NMR (600 MHz, CDCl₃): δ 6.96 (d, J = 8.7 Hz, 1H, -NH), 6.02 (d, J = 9.1 Hz, 1H, -NH), 5.86–5.82 (m, 2H), 5.80 (t, J = 7.2 Hz, 1H), 5.39–5.27 (m, 3H), 5.27–5.17 (m, 2H), 5.10–5.01 (m, 2H), 4.68 (d, J = 8.3 Hz, 1H, anomeric), 4.37–4.37 (m, 1H), 4.26–4.21 (m, 2H), 4.11 (dd, J = 12.3, 2.3 Hz, 1H), 3.98–3.91 (m, 1H), 3.91–3.81 (m, 1H), 3.84–3.78 (m, 1H), 3.74–3.65 (m, 3H), 2.58–2.39 (m, 2H), 2.41–2.28 (m, 2H), 2.08 (s, 3H), 2.04 (s, 3H), 2.03 (s, 5H, 3H × CH₃ and 2H -COCH₂), 2.02–1.99 (m, 2H), 1.97 (t, J = 2.5 Hz, 1H, acetylene), 1.65–1.52 (m, 2H), 1.37–1.20 (m, 49H), 1.19 (s, 9H), 1.11–1.01 (m, 1H), 0.88 (t, J = 7.0 Hz, 6H). ¹³C NMR (151 MHz, CDCl₃): δ 177.1, 171.8, 171.2, 170.7, 169.4, 157.2, 138.1, 123.7, 100.3, 82.7, 72.7, 72.3, 72.2, 69.5, 68.4, 65.4, 62.1, 54.5, 51.6, 39.0, 35.4, 33.0, 32.4, 32.0, 29.8, 29.8, 29.7, 29.6, 29.5, 29.5, 29.5, 29.2, 28.9, 27.1, 22.8, 20.8, 20.8, 20.7, 14.7, 14.2. HRMS (ESI-TOF) m/z: [M + H]⁺ Calcd for C₅₈H₉₉N₂O₁₂ 1043.7259; Found 1043.7269.

(2S,3R,E)-2-[11-(3-hexyl-3H-diazirin-3-yl)undecanamido]octadec-4-en-1-yl 2-deoxy-2-(pent-4-ynamido)-β-D-glucopyranoside (2)

To a solution of **11** (18 mg, 0.017 mmol) in dry MeOH/DCM (3:2, 2 ml) was added NaOMe in MeOH (4.5 M, 38.3 μl, 0.172 mmol) at 0°C. After the solution was stirred at rt for 2 days, the mixture was neutralized with Dowex 50W (H⁺) resin, filtered, and concentrated in vacuo. The product was purified by silica gel column chromatography to give **2** as a white solid (12.1 mg, 67%). TLC: R_f = 0.38 (CHCl₃/MeOH 4:0.5). ¹H NMR (600 MHz, MeOD:CDCl₃ 1:3): δ 5.66 (dt, J = 14.2, 6.7 Hz, 1H), 5.38 (dd, J = 15.3, 7.7 Hz, 1H), 4.31 (d, J = 8.3 Hz, 1H, anomeric), 4.06 (t, J = 7.8 Hz, 1H), 3.98 (dd, J = 10.1, 4.1 Hz, 1H), 3.93–3.79 (m, 2H), 3.75–3.57 (m, 3H), 3.40 (dd, J = 10.2, 8.7 Hz, 1H), 3.36–3.29 (m, 1H), 3.25 (ddd, J = 9.4, 6.0, 2.6 Hz, 1H), 2.55–2.33 (m, 5H), 2.18–2.10 (m, 1H), 2.09–2.03 (m, 1H), 2.02 (bs, 1H, acetylene), 2.01–1.89 (m, 2H), 1.59–1.49 (m, 2H), 1.48–1.13 (m, 46H), 1.06–0.99 (m, 1H), 0.86–0.81 (m, 6H). ¹³C NMR (151 MHz, MeOD): δ 175.0, 173.9, 134.8, 129.5, 101.4, 82.9, 76.5, 75.0, 71.9, 71.3, 69.5, 68.1, 62.0, 56.3, 53.6, 45.4, 36.8, 35.5, 33.2, 32.7, 32.2, 31.9, 30.1, 30.0, 30.0, 29.9, 29.8, 29.8, 29.8, 29.8, 29.7, 29.7, 29.7, 29.6, 29.6, 29.6, 29.5, 29.2, 26.3, 24.1, 24.1, 22.9, 22.8, 15.1, 14.2. HRMS (ESI-TOF) m/z: [M + H]⁺ Calcd for C₄₇H₈₅N₄O₈ 833.6362; Found 833.6382.

(2S,3R,E)-2-(tert-Butoxycarbonyl)amino-3-pivaloyloxyoctadec-4-en-1-yl 3,4,6-tri-O-acetyl-2-deoxy-2-(pent-4-ynamido)-β-D-galactopyranosyl-(1→3)-[3,4,6-tri-O-acetyl-2-deoxy-2-(pent-4-ynamido)-β-D-galactopyranosyl-(1→4)]-2,6-di-O-acetyl-β-D-galactopyranosyl-(1→4)-2,3,6-tri-O-acetyl-β-D-glucopyranoside (13)

Compound **13** (14.1 mg, 61%) was synthesized from **12** (27 mg, 0.016 mmol) by the same procedure and conditions employed for the synthesis of **9**. TLC: R_f = 0.7 (EtOAc). ¹H NMR (600 MHz, CDCl₃): δ 6.90 (d, J = 9.0 Hz, 1H, -NH), 5.89 (d, J = 7.8 Hz, 1H, -NH), 5.76 (dt, J = 14.3, 6.6 Hz, 1H, -C=CH), 5.39 (d, J = 3.0 Hz, 1H), 5.35 (d, J = 3.5 Hz, 1H), 5.33 (d, J = 7.3 Hz, 1H, -NH), 5.26 (d, J = 8.7 Hz, 1H, anomeric-H⁺), 5.21–5.16 (m, 2H), 5.11 (t, J = 9.5 Hz, 1H), 4.97–4.83 (m, 2H), 4.67 (d, J = 9.5 Hz, 1H, -NH), 4.55 (d, J = 8.0 Hz, 1H, anomeric-H⁺), 4.46–4.34 (m, 2H, anomeric-1H⁺), 4.30–4.08 (m, 8H, anomeric-1H), 4.09–3.99 (m, 3H), 3.99–3.81 (m, 4H), 3.70 (t, J = 9.5 Hz, 1H), 3.63 (dd, J = 10.0,

3.0 Hz, 1H), 3.61–3.58 (m, 1H), 3.57–3.54 (m, 1H), 3.47 (dd, J = 9.7, 4.4 Hz, 1H), 2.71–2.56 (m, 3H), 2.55–2.40 (m, 6H), 2.37–2.28 (m, 1H), 2.19 (s, 6H, 2 × CH₃), 2.12 (s, 3H), 2.10 (s, 3H), 2.07 (s, 3H), 2.06 (s, 3H), 2.05 (s, 6H), 2.02 (s, 3H), 2.02 (s, 3H), 2.00 (s, 3H), 1.97–1.95 (m, 2H), 1.41 (s, 9H), 1.35–1.21 (m, 22H), 1.16 (s, 9H), 0.88 (t, J = 7.0 Hz, 3H). ¹³C NMR (151 MHz, CDCl₃): δ 176.9, 174.0, 172.2, 172.1, 171.0, 170.9, 170.7, 170.6, 170.5, 170.3, 170.0, 169.8, 168.7, 155.3, 137.1, 124.6, 102.6, 101.2, 100.4, 100.1, 84.0, 83.2, 79.6, 79.1, 74.7, 73.2, 73.0, 72.4, 72.2, 71.8, 71.3, 71.2, 71.0, 70.6, 69.4, 69.3, 68.7, 68.6, 66.79, 66.6, 63.4, 62.3, 61.6, 61.0, 52.2, 51.5, 50.2, 38.9, 35.4, 35.0, 32.7, 32.4, 32.0, 29.8, 29.6, 29.62, 29.5, 29.3, 29.0, 28.4, 27.1, 22.8, 20.9, 20.9, 20.9, 20.8, 20.8, 20.7, 20.7, 14.9, 14.6, 14.3, 14.2. HRMS (ESI-TOF) m/z: [M + H]⁺ Calcd for C₈₄H₁₂₅N₃O₃₆ 1751.8116; Found 1751.8186.

(2S,3R,E)-2-[11-(3-hexyl-3H-diazirin-3-yl)undecanamido]-3-pivaloyloxyoctadec-4-en-1-yl 3,4,6-tri-O-acetyl-2-deoxy-2-(pent-4-ynamido)-β-D-galactopyranosyl-(1→3)-[3,4,6-tri-O-acetyl-2-deoxy-2-(pent-4-ynamido)-β-D-galactopyranosyl-(1→4)]-2,6-di-O-acetyl-β-D-galactopyranosyl-(1→4)-2,3,6-tri-O-acetyl-β-D-glucopyranoside (14)

Compound **14** (8.2 mg, 62%) was synthesized from **13** (12 mg, 0.006 mmol) by the same procedure and conditions employed for the synthesis of **11**. TLC: R_f = 0.7 (EtOAc). ¹H NMR (600 MHz, CDCl₃): δ 6.90 (d, J = 9.0 Hz, 1H, -NH), 5.85 (d, J = 7.9 Hz, 1H, -NH), 5.75 (dt, J = 14.4, 6.7 Hz, 1H, -C=CH), 5.63 (d, J = 9.3 Hz, 1H, -NH), 5.39 (d, J = 2.7 Hz, 1H), 5.36 (d, J = 2.6 Hz, 1H), 5.33 (d, J = 7.5 Hz, 1H), 5.25 (d, J = 8.6 Hz, 1H), 5.21 (t, J = 7.4 Hz, 1H), 5.19–5.15 (m, 2H), 5.12 (t, J = 9.5 Hz, 1H), 4.93–4.83 (m, 2H), 4.53 (d, J = 7.9 Hz, 1H, anomeric), 4.40 (d, J = 10.8 Hz, 1H), 4.38 (d, J = 7.8 Hz, 1H, anomeric), 4.35–4.30 (m, 1H), 4.29–4.10 (m, 8H), 4.08–3.99 (m, 3H), 3.94–3.86 (m, 3H), 3.70 (t, J = 9.6 Hz, 1H), 3.66–3.62 (m, 1H), 3.62–3.58 (m, 1H), 3.57–3.51 (m, 1H), 3.48 (dd, J = 4.5 Hz, 1H), 2.67–2.58 (m, 2H), 2.56–2.41 (m, 5H), 2.39–2.26 (m, 2H), 2.19 (s, 3H), 2.17 (s, 3H), 2.12 (s, 3H), 2.10 (s, 3H), 2.08 (s, 3H), 2.06 (s, 3H), 2.05 (s, 3H), 2.04 (s, 3H), 2.03 (s, 3H), 2.02 (s, 3H), 2.00 (s, 3H), 1.98–1.93 (m, 2H), 1.54–1.47 (m, 1H), 1.36–1.19 (m, 47H), 1.16 (s, 9H), 1.08–1.03 (m, 1H), 0.88 (t, J = 7.0 Hz, 6H). ¹³C NMR (151 MHz, CDCl₃): δ 177.0, 172.6, 172.1, 172.0, 171.0, 170.9, 170.7, 170.4, 170.2, 170.0, 169.8, 168.7, 168.6, 159.4, 159.3, 137.2, 125.0, 102.7, 100.9, 100.4, 100.0, 84.0, 83.2, 79.1, 73.1, 72.4, 72.2, 71.3, 71.1, 70.6, 69.4, 68.7, 68.6, 67.7, 66.6, 63.4, 62.3, 61.6, 61.0, 51.5, 50.5, 50.1, 38.9, 36.9, 35.4, 35.0, 34.8, 33.0, 32.4, 32.0, 31.7, 31.0, 29.8, 29.6, 29.5, 29.3, 29.3, 29.1, 29.0, 28.5, 27.1, 25.8, 25.4, 24.0, 22.8, 22.8, 21.2, 20.9, 20.9, 20.9, 20.8, 20.7, 20.7, 14.9, 14.6, 14.2, 14.1. HRMS (ESI-TOF) m/z: [M + H]⁺ Calcd for C₉₇H₁₄₉N₅O₃₅ 1944.0106; Found 1944.0197.

(2S,3R,E)-2-[11-(3-hexyl-3H-diazirin-3-yl)undecanamido]-3-hydroxyoctadec-4-en-1-yl 2-deoxy-2-(pent-4-ynamido)-β-D-galactopyranosyl-(1→3)-[2-deoxy-2-(pent-4-ynamido)-β-D-galactopyranosyl-(1→4)]-β-D-galactopyranosyl-(1→4)-β-D-glucopyranoside (1)

Compound **1** (4.1 mg, 69%) was prepared from **14** (8.2 mg, 0.004 mmol) by the same procedure and conditions used for the synthesis of **2**. TLC: R_f = 0.4 (MeOH:CHCl₃ 1:1). ¹H NMR (600 MHz, MeOD:CDCl₃ 1:1): δ 5.66 (dt, J = 14.3, 6.8 Hz, 1H), 5.42 (dd, J = 15.3, 7.6 Hz, 1H), 4.89 (d, J = 8.6 Hz, 1H, anomeric), 4.50 (d, J = 8.4 Hz, 1H, anomeric), 4.33 (d, J = 7.6 Hz, 1H, anomeric), 4.29 (d, J = 2.5 Hz, 1H), 4.25 (d, J =

7.7 Hz, 1H, anomeric), 4.16 (dd, $J = 9.9, 4.1$ Hz, 1H), 4.05 (t, $J = 7.8$ Hz, 1H), 3.96–3.90 (m, 3H), 3.86–3.76 (m, 7H), 3.73–3.66 (m, 2H), 3.64 (dd, $J = 11.6, 5.6$ Hz, 1H), 3.62–3.57 (m, 2H), 3.57–3.46 (m, 8H), 3.34 (ddd, $J = 10.2, 4.9, 2.4$ Hz, 1H), 3.29–3.26 (m, 1H), 2.56–2.38 (m, 8H), 2.14 (t, $J = 7.6$ Hz, 2H), 2.10–2.06 (m, 2H), 2.02–1.96 (m, 2H), 1.60–1.51 (m, 2H), 1.43–1.14 (m, 46H), 1.08–1.00 (m, 2H), 0.85 (t, $J = 7.0$ Hz, 3H). ^{13}C NMR (151 MHz, MeOD): δ 174.7, 154.8, 154.7, 134.9, 129.9, 104.2, 104.0, 103.5, 102.3, 83.6, 83.4, 79.2, 75.8, 75.7, 75.5, 75.15, 74.5, 73.9, 73.1, 72.5, 72.4, 70.3, 69.6, 69.5, 69.2, 69.1, 68.9, 62.3, 62.2, 61.0, 60.5, 54.2, 53.9, 53.8, 53.4, 36.9, 35.5, 33.3, 32.8, 32.4, 30.1, 30.1, 30.0, 29.9, 29.8, 29.7, 29.3, 28.6, 26.4, 24.32, 24.2, 23.1, 22.9, 15.1, 14.2. HRMS (ESI-TOF) m/z : $[\text{M} + \text{H}]^+$ Calcd for $\text{C}_{70}\text{H}_{119}\text{N}_5\text{O}_{23}$ 1398.8369; Found 1398.8416.

Cell culture

HEK293 cells were cultured in high glucose DMEM supplemented with 10% (V/V) FBS, 100 $\mu\text{g}/\text{ml}$ streptomycin, and 100 U/ml penicillin at 37°C in a 5% CO_2 incubator maintaining a water-saturated atmosphere. HEK293 cells of passage four were used for various studies.

Fluorescence imaging of cells

HEK293 cells (50×10^3) were seeded in poly-L-lysine (1% solution in DPBS)-coated 35 mm dish and were allowed to grow to ~60% confluence. Cells were washed three times with DPBS and incubated with RPMI buffer (1 ml) containing 50 μM of **2** (24.43 μl from 2.05 mM stock solution in DMSO) or **1** (18.94 μl from 2.64 mM stock solution in DMSO), respectively. For the negative control, cells were incubated with DPBS only. After 3 h of incubation, cells were washed with DPBS (0.5 ml) three times, and DPBS (1 ml) was added to each dish. Cells were exposed to UV irradiation (365 nm wavelength) at 4°C for 15 min using a Spectroline UV lamp (Spectroline, ENF-280C, 120 V, 60 Hz, 0.20 Amps), which was followed by washing. Cells were incubated with 4% PFA in DPBS at rt for 15 min and rinsed with DPBS (3×1 ml). The fixed cells were treated with click master mix (50 μM Biotin-Azide, 50 mM THPTA, 4.75 mM sodium ascorbate, and 2 mM CuSO_4) at rt for 1 h as described in the literature (60). Cells were washed with DPBS (3×500 μl), 500 mM aq. NaCl solution (3×500 μl), and double-distilled water. Cells were incubated with streptavidin-A488 (1:1,000 dilution of 1 mg/ml stock) in 1 ml of DPBS for 30 min in the dark. After washing with DPBS, cells were incubated with DAPI (50 nM, 1 ml for each dish) at rt for 5 min. Finally, the cells were washed with DPBS and subjected to fluorescent imaging.

For organelle localization study, HEK293 cells were treated with streptavidin-A488 by the same procedure. The cells were washed, fixed, and permeabilized with cell permeabilization buffer for 15 min, followed by washing and incubation with fluorophore-conjugated organelle antibody markers (in a final concentration of 2 $\mu\text{g}/\text{ml}$ for each antibody) in 1 ml of DPBS containing 1.5% BSA at rt for 1 h with gentle shaking. Finally, the coverslip containing cells was washed and mounted on the microscopic glass slide using the mounting media.

Flow cytometry analysis of cells

After treatment with **1** or **2** (200 μM), using DPBS as control, for different periods (1, 2, 3, 4, 6, and 12 h), cells were pelleted by centrifugation (600 g) at 4°C for 8 min, suspended in DPBS (1 \times , 200 μl) containing 100 μM of biotin-azide, and incubated

on ice for 45 min as mentioned above. Cells were washed with ice-cold PBS (1.0 ml) and pelleted by centrifugation, which was repeated three times. The cells were suspended in PBS (100 μl) and incubated with A488-streptavidin (1:500 dilution) on ice in the dark for 30 min. The cells were centrifuged and washed with ice-cold DPBS (500 μl), which was repeated three times. Finally, the cells were resuspended in ice-cold PBS (200 μl) and subjected to FACS analysis using a blue (488 nm) excitation laser and 530 nm emission filter. Data were analyzed using the Attune NXT software.

Labeling proteins in live HEK293 cells using **1** and **2**

HEK293 cells (0.8×10^6) were seeded onto a 100 mm tissue culture dish as mentioned above and were allowed to grow to 90% confluence. The cells were harvested, pelleted, and resuspended in serum-free media (7 ml) with a final cell count of $\sim 4.7 \times 10^6$. Cells were equally divided into three centrifuge tubes, washed with DPBS three times, replenished with fresh serum-free media containing 200 μM of **1**, **2**, or PBS (negative control), and transferred onto a 35 mm tissue culture dish. Following incubation at 37°C for 4 h, cells were washed with DPBS, resuspended in DPBS (1 ml), and exposed to 365 nm UV light as described. Thereafter, cells were pelleted through centrifugation (800 g , 4°C, 6 min), washed with cold DPBS (2 \times), and aspirated. Cell pellets were either stored at -80°C until use or directly applied to the next step.

Western blot analysis of labeled proteins

These experiments followed our previous protocols (60, 61). In short, the cell pellets obtained above were lysed in ice-cold lysis buffer (500 μl) containing 5.0 μM protease inhibitor (Halt protease inhibitor cocktail, Thermo Scientific) on a Qsonica probe sonicator (6 pulses, 60% duty cycle, 30 s each, Amp 10). The whole cell lysate (WCL) was subjected to protein precipitation by adding cold MeOH (2 ml), CHCl_3 (0.5 ml), and water (3.5 ml) (4/1/7, v/v/v), followed by mixing and centrifuging at 21,000 g for 20 min. The supernatant was discarded, and this precipitation process was repeated two more times. The resulting protein pellet was dried at rt, resuspended in PBS, and analyzed to determine protein concentration using a bicinchoninic acid (BCA) protein assay kit (Thermo Scientific) following the manufacturer's instructions. An aliquot of ca. 50 μg proteins was put in a 1.5 ml centrifuge tube and mixed with freshly prepared click master mix (50 μM Biotin-Azide, 50 mM THPTA, 4.75 mM sodium ascorbate, and 2 mM CuSO_4) at rt for 1 h. Each reaction mixture was made up to 50 μl of final volume by adding DPBS and mixed by vortexing. The reaction was kept at rt for 1 h before being quenched with 50 μl ice-cold MeOH. Cold DPBS (50 μl) was added to the mixture, followed by cold MeOH (150 μl), CHCl_3 (50 μl), and water (300 μl). The cloudy solution was vortexed and then centrifuged (21,000 g , 4°C, 20 min) to separate proteins from the aqueous and organic layers, and the protein fraction was washed with cold MeOH (3 \times). The pelleted proteins were dried at rt, resuspended in SDS lysis buffer (100 μl), and sonicated in a water bath until they were dissolved. Protein concentration was measured using a BCA protein assay kit. Proteins (25 $\mu\text{g}/\text{gel}$ lane) were mixed with SDS loading buffer (4 \times stock), boiled at 95°C, loaded in SDS-PAGE gels containing 10% acrylamide, and developed. The protein gel was transferred onto the PVDF membrane that was washed with PBS, incubated with blocking solution (10 ml) at rt for 1 h, washed with PBS again, and then incubated with streptavidin-alkaline phosphatase (AP) (1 $\mu\text{g}/\text{ml}$ in PBS) at rt for 45 min with gentle shaking. The membrane was

washed with PBS, and the protein bands were detected by incubating with 5-bromo-4-chloro-3-indolyl phosphate (BCIP)/nitro blue tetrazolium (NBT) chromogenic substrate (1 tablet dissolved in 7 ml of PBS) for 5 min before being photographed.

MS/MS-based proteomic analysis

Cell lysis, tagging of the labeled proteins with biotin using biotin-azide instead of Cy5-azide for the click reaction, and protein isolation from cell lysate followed the above-described protocols. The protein fractions were washed with MeOH, pelleted, and then resuspended in a freshly prepared pre-equilibrated solution of streptavidin Agarose resin in DPBS (300 μ l) at rt for 2 h with end-to-end rotation. The streptavidin beads were separated by centrifugation (1,500 g, 2 min) and washed with 0.2% SDS in DPBS (3 \times 2 ml) and H₂O (3 \times 2 ml). The beads were finally applied to an MS/MS-based proteomic study. MS sample preparation and analysis conditions are the following. 1) On-bead trypsin digestion of proteins. Protein-loaded beads obtained above were diluted with 50 mM ammonium bicarbonate and then treated with 4 mM dithiothreitol (DTT) at 65°C for 15 min, 10 mM chloroacetamide (CAA) at rt for 30 min in the dark. Next, the beads were treated with trypsin (500 ng) at 37°C overnight. Tryptic peptides were desalted with ZipTip following the manufacturer's protocol (Millipore Sigma). The peptides were lyophilized at 160 mBar with a speed vac and resuspended in 0.1% formic acid (FA) for liquid chromatography-tandem mass spectrometry (LC-MS/MS) analysis. Two valid replicates for each genotype were prepared for proteomic study. 2) LC-MS/MS-based proteomic study. Proteomic data acquisition was achieved on an EASY-nLC™ 1200 System coupled with Orbitrap Fusion™ Mass Spectrometers (Thermo Fisher Scientific). Samples were loaded to a PepMap® 100 C18 trapping column (75 μ m i.d. \times 2 cm, 3 μ m, 100 Å) and separated on a PepMap® C18 analytical column (75 μ m i.d. \times 25 cm, 2 μ m, 100 Å). The flow rate was set at 250 nl/min with solvent A (0.1% FA in water) and solvent B (0.1% FA and 80% acetonitrile in water) as the mobile phases. Separation was conducted using the gradient of 2%–35% of B over 0–70 min; 35%–80% of B over 70–75 min; 80%–98% of B over 75–76 min, and isocratic at 98% of B over 76–90 min. For MS data acquisition, the full MS1 scan (*m/z* 350–1,800) was performed on the Orbitrap with a resolution of 120,000. The automatic gain control (AGC) target is 2e5 with a maximum injection time of 50 ms. Peptides bearing +2–6 charges were selected with an intensity threshold of 1e4. Dynamic exclusion of 30 s was used to prevent resampling the high abundance peptides, and the quadrupole isolation window was 1.3 Th. Fragmentation of the top 10 selected peptides by collision-induced dissociation was done at 35% of normalized collision energy. The MS2 spectra were acquired at the Ion Trap with AGC target as 1e4 and maximum injection time as 35 ms.

Analysis of MS/MS data

Proteome Discoverer™ (version 2.5, Thermo Scientific) was used to search the MS/MS spectra from the protein samples. The SEQUEST algorithm in the Proteome Discoverer was used to process raw data. Spectra were searched using the Uniprot *Homo sapiens* protein database with the following parameters: 10 ppm mass tolerance for MS1 and 0.6 for MS2, two maximum missed tryptic cleavage sites, a fixed modification of carbamidomethylation (+57.021) on cysteine residues, and dynamic modifications of oxidation of

methionine (+15.996). Search results were filtered at 1% false discovery rate (FDR) and at least two unique peptides per protein for protein identification. Relative protein abundance in the samples was measured using label-free quantification, and proteins identified and quantified in all biological samples were used. No imputation was performed. Peptides in samples were quantified as areas under the chromatogram peak. FDR cutoffs for both peptide and protein identification were set as 1%.

Experimental validation of candidate GSL-binding proteins

HEK293 cells ($\sim 0.8 \times 10^6$) were seeded in a poly-L-lysine-coated 60 mm tissue culture dish with 5 ml of cell culture media and grown until $\sim 80\%$ confluence for transfection. The transfection reagent was prepared according to the manufacturer's protocols using the recommended concentration of lipofectamine agent. In short, on the day of transfection, 2.5 μ g of plasmid DNA was diluted in 600 μ l of OptiMEM media, and 10 μ l of lipofectamine 2000™ transfection reagent was separately diluted in 600 μ l of OptiMEM media containing enhancer reagent (2 μ l). The two solutions were mixed and incubated at rt for 45 min with occasional mixing using a pipette. In the meantime, cells were washed with OptiMEM media (1 ml) three times and incubated with the DNA/lipofectamine reagent mixture in 2.5 ml of OptiMEM media for 5 h. Thereafter, 2.5 ml of serum-containing cell culture media was added to the cells. After 12 h of incubation, the cell culture media was discarded and replenished with 5 ml of serum-containing media for 36 h. The transfection efficiency was validated and optimized by analyzing the proteins extracted from the WCL using SDS-PAGE as mentioned above and blotting against the anti-protein antibody or anti-FLAG tag antibody. The generated transfected cells were incubated with 1, 2, or PBS (control) and then exposed to UV irradiation following the protocol mentioned above. Cells were collected by centrifugation, washed with cold DPBS, and lysed by resuspending the pellet in 1 ml of cell lysis buffer containing 10 μ l of protease inhibitor cocktail using a Qsonica probe sonicator (6 pulses, 60% duty cycle, 30 s each, Amp10). Cell lysate was subjected to protein extraction following the above protocol. Protein pellet was resuspended in DPBS, and protein concentration was measured using a BCA assay kit. Proteins (~ 500 μ g) were placed in a separate centrifuge tube and subjected to click reaction with biotin-azide as mentioned above. The reaction was quenched by adding cold methanol, and the proteins were extracted. The protein pellet was resuspended in DPBS with protein concentration measured with a BCA assay kit. Thereafter, ~ 250 μ g of proteins was diluted in cell lysis buffer (final volume of 300 μ l) and subjected to anti-FLAG magnetic agarose bead-mediated purification according to the manufacturer's protocol. Thus, 50 μ l of the magnetic bead slurry (25% slurry stock dissolved in DPBS containing 0.01% Tween-20 and 0.02% sodium azide, pH 7.2) was transferred into a 1.5 ml centrifuge tube and washed with cell lysis buffer (450 μ l) three times. The tube was placed on a magnetic stand to collect the beads while discarding the supernatant. This bead-washing process was repeated four more times. Next, protein samples (300 μ l) were added to the washed beads, followed by vortexing and incubation at rt for 45 min. The beads were collected with a magnetic stand and washed with cell lysis buffer three times and protein washing buffer (1 \times

DPBS containing 150 mM NaCl, pH 7.2) three times. Thereafter, 50 μ l of SDS-PAGE buffer containing 2.5 μ l of 2M DTT was added to each tube, and the sample was heated at 95°C for 15 min. The magnetic beads were separated from the solution using a magnetic stand. An aliquot of the supernatant was subjected to SDS-PAGE and Coomassie blue staining for visualization, whereas another aliquot of the supernatant (~25 μ l) was subjected to SDS-PAGE and fluorescence analysis employing Cy5-streptavidin conjugate solution (1 μ g/ml in DPBS) according to conventional protocols.

Statistical analysis

Statistical analysis of data was achieved with the GraphPad Prism 9.0 software. Results are presented as the mean \pm standard deviation and are compared with a two-tailed student's *t* test. **P* < 0.05, ***P* < 0.01, ****P* < 0.001, and *****P* < 0.0001 show different levels of statistical significance.

RESULTS

Research design

To study GSL-cell membrane interactions and identify GSL-binding membrane proteins, it is necessary to have probes that not only label GSL-binding proteins but also help isolate them. In this context, we have designed and synthesized bifunctional derivatives **1** and **2** (Fig. 2) of II³- β -(*N*-acetyl-D-galactosamine)-GA2 (GalNAc-GA2), which is an epimer of LcGg4, and β -(*N*-acetyl-D-glucosamine)-ceramide (GlcNAc-Cer), respectively. The latter is utilized as a negative control because GlcNAc-Cer linkage is not found in mammalian GSLs yet. However, these two probes contain the same lipid tail, which carries a photoreactive diazirine in the fatty acyl moiety that can be activated with 365 nm UV light to yield a carbene to react with proximal molecules and generate a covalent linkage. This will enable **1** and **2** attachment to transmembrane proteins close to or interacting with their lipid moiety and, hence, label the targeted

proteins. Photo-affinity labeling has proved to be a powerful tool to investigate protein-protein/lipid interactions in live cells (62–66). The C18:0 stearic group in **1** and **2** is an abundant fatty acyl chain in the Cer moiety of mammalian GSLs, while its C-12, where the diazirine is located, would be in the outer leaflet of the cell membrane. In the meantime, both **1** and **2** also contain alkynes in the glycan, which can react with azides via click reactions under mild conditions for the introduction of an affinity tag to facilitate the rapid isolation of crosslinked proteins and subsequent proteomic studies. Probe **1** was designed to contain an alkyne group in each GalNAc unit, as its synthesis is easier than that of probes with alkyne on a single GalNAc residue, which needs to differentiate the two sugar units. The diazirine and alkyne groups are used to modify the fatty acyl chain of Cer and the GalNAc *N*-acetyl group of glycans, respectively, because they are small and are expected to have a minimal impact on the GSL structure. Thus, **1** and **2** are anticipated to be effective probes to explore GSL-membrane interaction, while the exact impact of the pent-4-ynoic group on GSL-membrane interactions can be studied by comparing **1** to probes containing unmodified glycans. Moreover, probes **1** and **2** are designed to have the diazirine and alkyne moieties separately located in the lipid and glycan. As a result, even if **1** and **2** are metabolized and their metabolites are incorporated by cells into the salvage biosynthetic pathways of GSLs and other biomolecules like lipids or glycoproteins, it is unlikely that both functional groups would end up in the same biosynthetic products for being labeled and pulled down simultaneously. Additionally, because **1** and **2** contain the same Cer moiety but different glycans, comparing the proteins captured by these probes can provide additional information. Firstly, the results will verify the feasibility of these probes to label and identify GSL-associated membrane proteins. Secondly, the results will demonstrate how the glycan structure

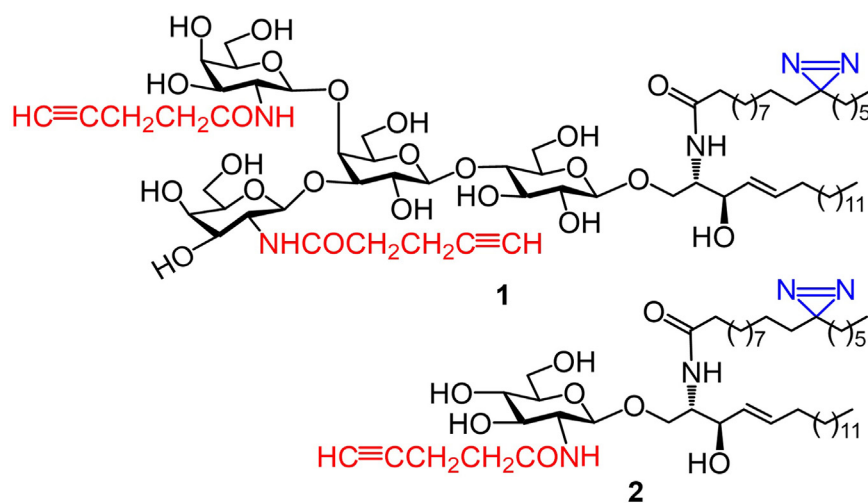


Fig. 2. Structures of the designed GSL probes **1** and **2**.

in GSLs influences their interactions with cell membranes and other functions.

Our experimental procedures/protocols for the labeling, pull-down, and identification of GSL-interacting membrane proteins are depicted in **Fig. 3**. Synthetic probes **1** and **2** will be added to the cell culture for cellular incorporation into membranes, which has been verified with many synthetic glycolipids (60, 61, 67, 68). Next, the cells will be subjected to UV irradiation to initiate the cross-linkage between probes and adjacent or GSL-interacting membrane proteins, thereby labeling the targeted proteins. Subsequently, total proteins will be extracted from the cell lysates and applied to a click reaction to attach a biotin tag to the crosslinked proteins. Finally, the biotinylated proteins will be isolated with streptavidin-beads and subjected to MS/MS-based proteomic analysis by conventional protocols.

Chemical synthesis of probes **1** and **2**

The synthesis of probe **2**, as outlined in **Scheme 1**, commenced with the conversion of a fully protected glucosamine derivative **3** into imidate **4** as a glycosyl donor in two steps, including regioselective anomeric de-O-acetylation using hydrazine acetate and reaction of the resultant hemiacetal with trichloroacetonitrile in the presence of 1,8-diazabicyclo[5.4.0]undec-7-ene

(DBU) under conventional conditions. Glycosylation of the sphingosine precursor **5** with **4** under the promotion of TMSOTf gave an excellent overall yield (88% for three steps) of the glycolipid precursor **6**. The newly formed β -glycosidic linkage in **6** was confirmed by the large coupling constant ($J = 7.5$ Hz) of the anomeric ^1H signal (δ 4.59 ppm) in its ^1H NMR spectrum. Thereafter, **6** was subjected to lipid remodeling and protecting group manipulation. Firstly, cross-metathesis of **6** and *n*-pentadecene **7** in the presence of the second-generation Hoveyda-Grubbs catalyst (3 mol%) in DCM gave the desired *Z*-olefin **8** (82%), which was confirmed by the coupling constant ($J = 15.3$ Hz) of its vinyl protons. This reaction was slow, taking approximately 5 days to complete, but clean. Next, the *N*-2,2,2-trichloroethoxycarbonyl (Troc) group in **8** was selectively removed using Zn/AcOH, which was followed by selective *N*-acylation of the resultant amine using 4-pentynoic acid and EDC to provide **9** in a 71% yield (two steps). The successful incorporation of an alkyne group in **9** was verified by its ^1H NMR spectrum, showing the terminal alkyne proton as a triplet ($J = 2.5$ Hz) at δ 1.99 ppm. Subsequently, the *N*-*tert*-butyloxycarbonyl (Boc) group in **9** was removed with 4% TFA in DCM, and the resultant amine was acylated using C-12-diazirine-modified stearic acid **10** (67, 68), EDC, and DMAP to provide **11** in

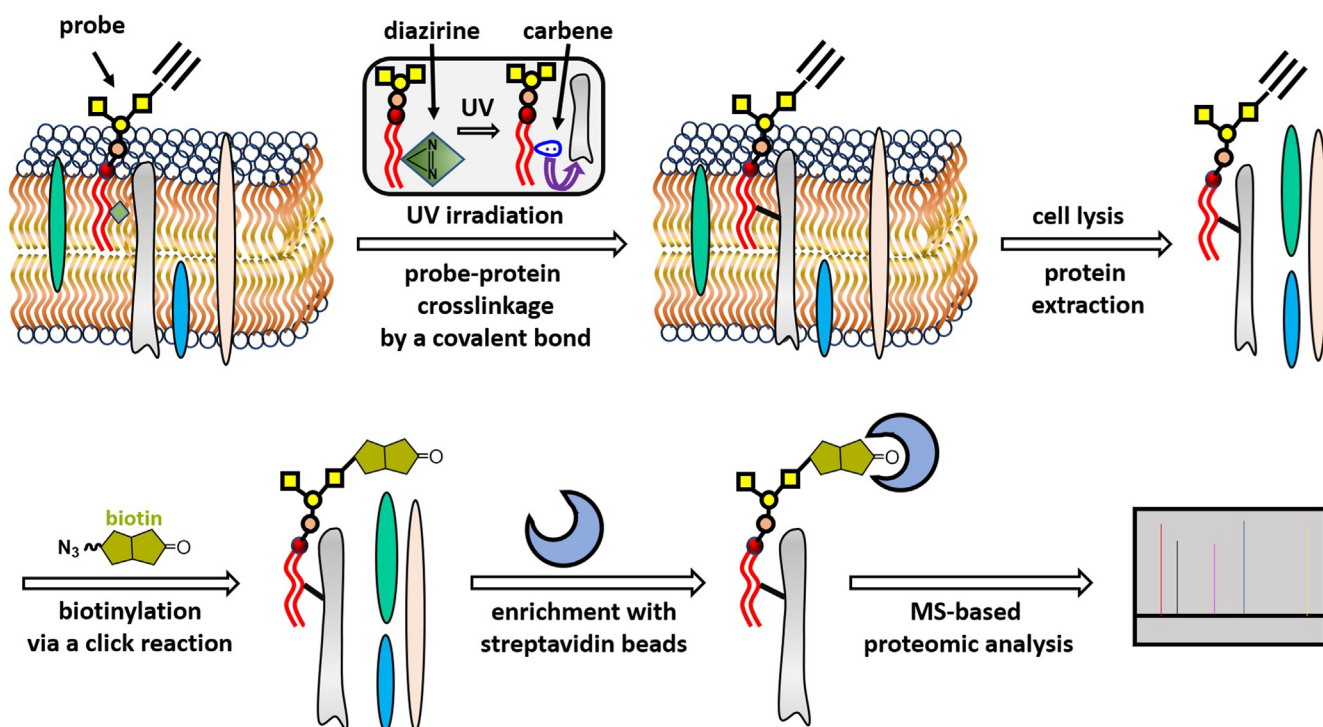
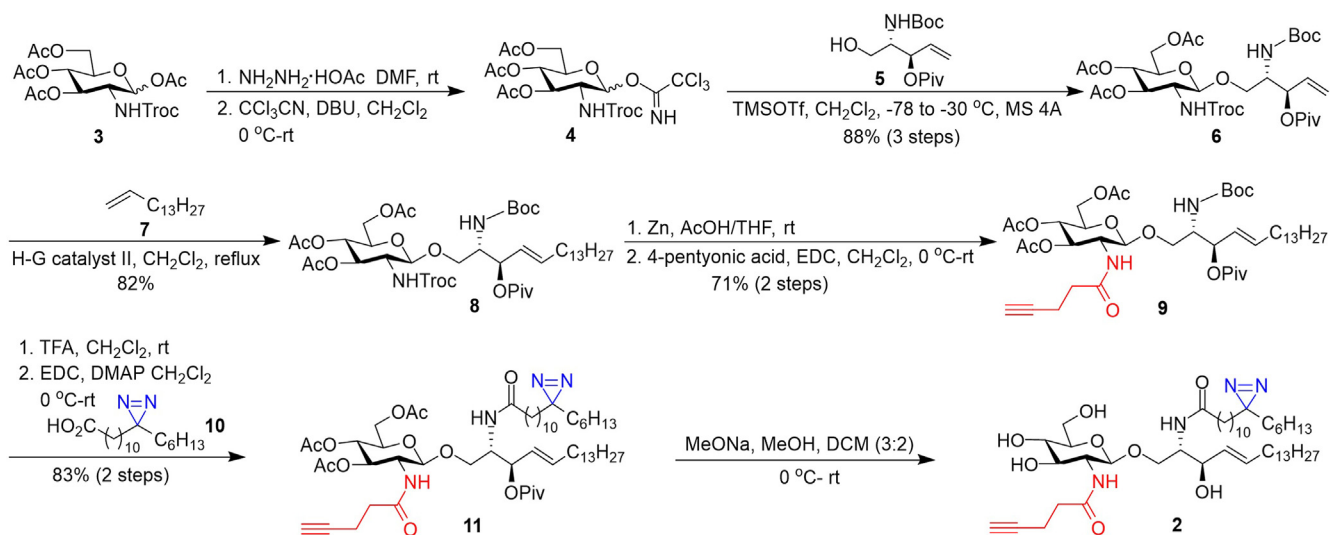


Fig. 3. An illustration of the experimental procedures designed to label and isolate GSL-interacting proteins in the cell membrane for proteomic study. Synthetic GSL probes are spontaneously integrated into the cell membrane after incubation with cells. Upon UV irradiation of the cells, a reactive carbene is generated in the lipid chain of the probe, which reacts with proteins nearby to form a covalent bond. Click reaction between the alkyne group in the probe and azide-modified biotin labels the crosslinked proteins with a biotin tag to facilitate their isolation utilizing streptavidin-modified beads. The bead-bound proteins are subjected to MS/MS-based proteomic analysis according to established protocols.



Scheme 1. Synthesis of probe **2**.

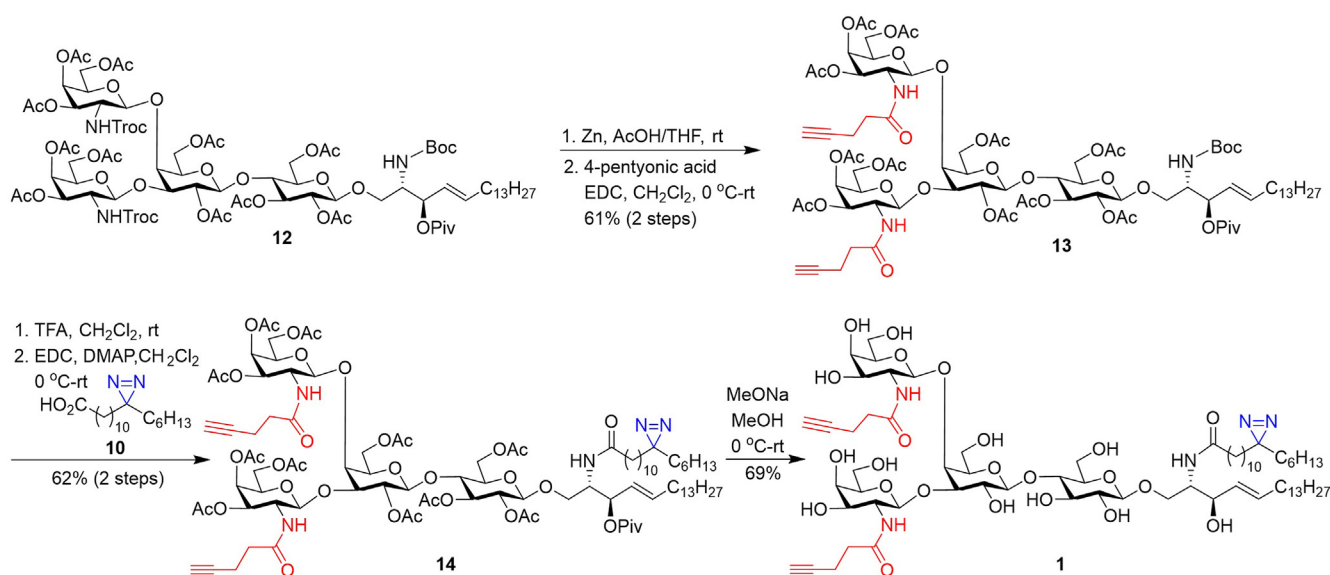
an 83% yield. Finally, all *O*-acyl groups in **11** were removed with NaOMe (5 M) to afford **2** in a 67% yield. The diazirine moiety was proved to be stable to the deprotection conditions.

Probe **1** was synthesized by the procedure outlined in [Scheme 2](#). First, we prepared the key intermediate **12** according to a method developed for the synthesis of LcGg4 and its derivatives (69). Next, as described above, the *N*-Troc groups in **12** were selectively removed using Zn/AcOH, which was followed by *N*-acylation using 4-pentynoic acid, EDC, and DMAP to provide **13** in a 61% yield. Similarly, the diazirine-modified fatty acyl chain was attached to the lipid moiety using **10** in the presence of EDC and DMAP, after the Boc group in **13** was removed with TFA, to afford **14**. Finally, global deprotection of **14** with NaOMe provided **1** in a good yield (69%). Both **1** and **2**, as well as the synthetic

intermediates, were fully characterized with NMR and HRMS data.

Cell incorporation of probes **1** and **2**

The human embryonic kidney (HEK) 293 cell was used in this study since it has been commonly used for protein overexpression and related studies and its proteomic information is easily accessible (70). For example, currently, there are several reports about quantitative and qualitative proteomics (71, 72) and GSL analyses (73) of HEK293 cells. To verify the effective incorporation of **1** and **2** in HEK293 cell membranes, we performed fluorescence labeling and flow cytometry (FACS) study of cells. In these experiments, HEK293 cells were incubated with **1** and **2** for different periods (1–12 h) and washed. Then, the cells were



Scheme 2. Synthesis of probe **1**.

sequentially treated with azide-modified biotin for biotinylation by copper-catalyzed alkyne-azide cycloaddition (CuAAC), a click reaction, and streptavidin-A488 (a green fluorophore). Finally, fluorescence intensities of the treated cells were analyzed with FACS to prove that **1** and **2** were efficiently incorporated by HEK293 cells within 2–3 h (supplemental Fig. S1). No further significant increase in the fluorescence intensity was observed after 12 h of incubation, which agreed with previous reports (61, 74). We also utilized fluorescence microscopy to validate the incorporation of **1** and **2** by HEK293 cells. To this end, cells were incubated with the probes for 3 h, washed, exposed to UV lights for 15 min, and then treated with azide-modified biotin and streptavidin-A488 as described. Finally, the labeled cells were analyzed using a fluorescence microscope. The results (Fig. 4A) clearly show strong fluorescent labeling of cells treated with both **1** and **2**, in contrast to control cells treated with PBS instead. Therefore, both the FACS and fluorescence microscopy results indicate the efficient incorporation of **1** and **2** into the membranes by HEK293 cells.

Previous studies by our group and others indicate that besides the plasma membrane, glycolipids can also translocate into cells to interact with intracellular organelle membranes (60, 61, 75–77). To determine the locations of **1** and **2** in organelles, we studied their cellular distributions using fluorescence labeling. After cells were incubated with **1** or **2** for 1, 2, 3, and 4 h and

labeled with azide-biotin and streptavidin-A488, they were fixed, permeabilized, and treated with A647-tagged anti-calreticulin, GM130, EEA1, RAB7, and LAMP1 antibodies to stain the endoplasmic reticulum (ER), Golgi, early endosome, late endosome, and lysosome (supplemental Table S1), respectively. Next, the cells were analyzed with a fluorescent microscope using the A488 and Cy5 channels to find the correlation between the two fluorescent labels. The results (supplemental Figs. S2–S11) reveal a time-dependent colocalization of **1** or **2** with intracellular organelles. Within 1 h, both **1** and **2** showed a significant overlap with ER fluorescence, suggesting their rapid incorporation into ER, which is the main destination in GSL recycling. However, such correlation declines with elongated time, possibly due to probe metabolism and redistribution to other organelles. Indeed, the correlation of **1** or **2** with other organelles is low at 1 h but increases gradually until 3 h, followed by a generally declining trend thereafter, especially for **1**. Interestingly, the overlap of both **1** and **2** with lysosome is low. These findings are further validated by the results of Pearson correlation coefficient analysis (supplemental Figs. S12 and S13). Moreover, **1** and **2** show different distributions in specific organelles, suggesting their potentially different transport and metabolism pathways due to their different glycans. Since the two probes show the most similar localization patterns at 3 h, this condition was selected for subsequent

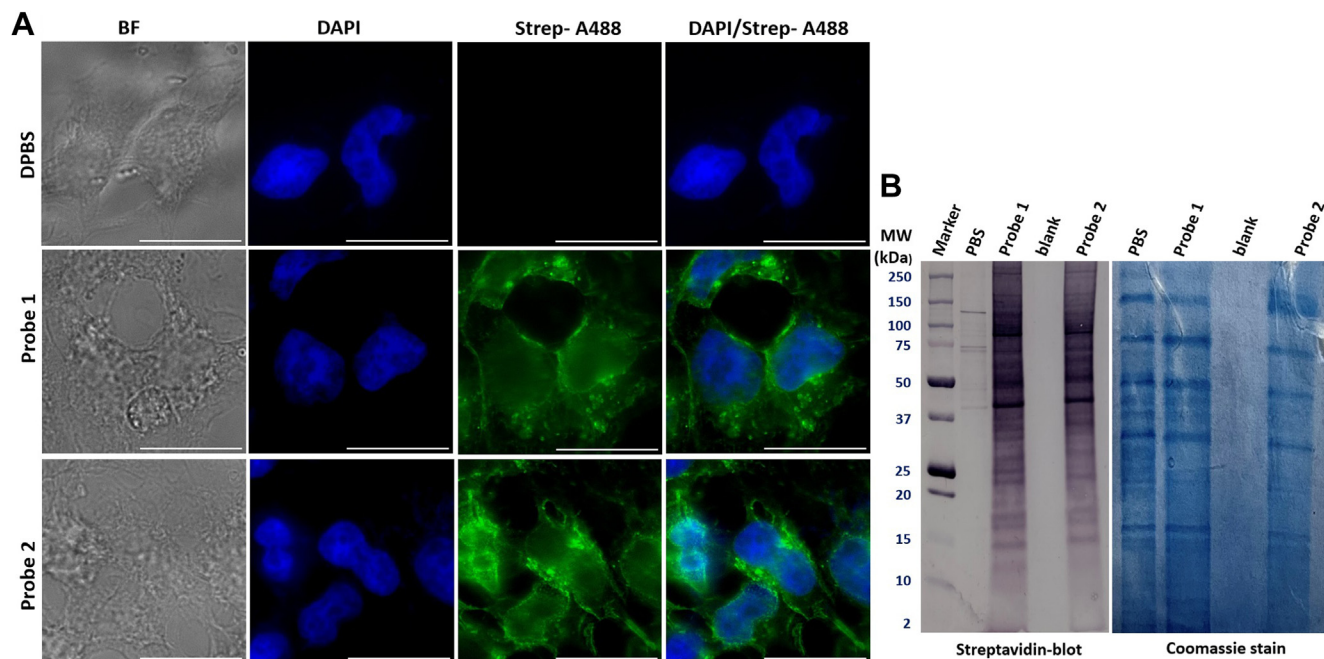


Fig. 4. A: Bright-field (BF), 4',6-diamidino-2-phenylindole (DAPI), streptavidin-A488 (Strep-A488), and Strep-A488/DAPI overlay fluorescent images of HEK293 cells treated with DPBS (negative control), **1**, and **2**, respectively, followed by treatments with azide-modified biotin, Streptavidin-A488, and finally DAPI to stain DNAs in the cell nucleus. The scale bar is 20 μ m. B: Western blot (left) and Coomassie blue staining (right) results of proteins extracted from HEK293 cells treated with **1**, **2**, or DPBS buffer (negative control), then with biotin-azide, and finally run by SDS-PAGE and stained with streptavidin-AP and then with BCIP/NBT (left) or Coomassie blue (right).

experiments. Clearly, upon incubation with cells, at least a part of **1** and **2** is localized in intracellular organelles, which is expected due to their involvement in glycolipid metabolism and recycling (77, 78). Thus, crosslinking of these probes with proteins in intracellular membranes is also expected in the following experiments. In addition, we cannot eliminate the possibility that some fluorescent signals are from other biomolecules that have incorporated alkyl GlcNAc in the metabolites of **1** and **2** through salvage pathways, but unlike **1** and **2**, they are not bifunctional to achieve simultaneous cross-linkage with membrane components and biotinylation in subsequent experiments.

Analysis of GSL-interacting membrane proteins in live cells using probes **1** and **2**

Next, we conducted experiments to investigate whether **1** and **2** could crosslink with proteins in live cells for protein pull-down and analysis. Following the procedure outlined in Fig. 3, we incubated HEK293 cells with **1** or **2** for 3 h and then exposed the cells to UV lights to allow for probe-protein crosslinking. Thereafter, the cells were lysed, and the proteins were extracted. An aliquot of the protein sample was subjected to a click reaction with azide-modified biotin to introduce a biotin tag to the probes. Finally, the proteins were precipitated to remove excess biotin and applied to sodium dodecyl sulfate-polyacrylamide gel electrophoresis (SDS-PAGE). The developed gels were treated with streptavidin-AP and BCIP/NBT for the detection of biotinylated proteins. The results (Fig. 4B) clearly indicate that both probes can label and pull down many proteins, which contrasts cells treated with only DPBS (negative control), suggesting the feasibility of using **1** and **2** to investigate GSL-membrane interactions.

Analysis of GSL-interacting proteins in the membranes of HEK293 cells was performed according to the procedure depicted in Fig. 3, using the optimized conditions established by the SDS-PAGE study. After incubation of cells with the probes and UV irradiation, cells were lysed, and the cell lysates were subjected to protein precipitation, click reaction with biotin-azide, and then protein precipitation as described earlier. The proteins were dissolved in SDS buffer and incubated with streptavidin beads. The beads were isolated, washed, and finally subjected to MS/MS-based proteomic analysis following well-established protocols. Each experiment was repeated three times to verify the results.

Our proteomic results reveal 2,584 proteins (supplemental Fig. S14) identified with **1** (2,272 proteins) and **2** (2,284 proteins). The volcano plot of proteins pulled down by **1**, using proteins pulled down by **2** as references, is depicted in Fig. 5A. Among the 2,584 proteins, 1,972 are common for **1** and **2**, and 312 are unique for **1**. Of the 312 unique proteins (supplemental Table S2), 238 were observed in all three experiments,

while the other 74 proteins were observed in any two experiments (supplemental Fig. S15). In addition to the unique proteins, we have also identified 65 proteins significantly enriched with **1** (supplemental Table S3). In the meantime, we have identified 300 proteins specific for **2** (i.e., not crosslinking to **1**), of which 105 were observed in all three experiments (supplemental Table S4). Overall, many proteins are crosslinked with probes **1** and **2**. Nonetheless, each probe can selectively interact with a specific set of proteins, even though the two probes have the same lipid moiety. These results suggest the significant influence of the glycan structure of GSLs on their interaction with the cell membrane. The unique and highly enriched proteins identified with **1** and **2** should be useful targets for further in-depth investigation of GSLs as well as their signaling and metabolic pathways.

The identities of the 238 unique proteins pulled down by **1**, along with their cellular locations and potential biological functions, were analyzed in detail (supplemental Table S1). According to the Uniprot data, most of these proteins are associated with membranes, either plasma or intracellular organelle membranes. As anticipated, **1** and **2** target not only the plasma membrane but also the ER, Golgi, and nuclear membranes, because glycolipids can be internalized by cells via varied mechanisms. Optimizing the time of cell incubation with probes may help gain certain selectivity, according to the results in supplemental Figs. S2–S13. Nevertheless, cell internalization does not affect **1** and **2** as useful probes to explore GSL-cell membrane interactions; instead, it can broaden the application scope of these probes, for example, for the characterization of proteins related to GSL biosynthesis, transport, recycling, and trafficking, which is one of our future research directions.

More importantly, a series of the unique proteins pulled down by **1** (Table 1) are reported or predicted to be related to GSLs, including GSL endocytosis, trafficking, and GSL-mediated signaling. For example, the vacuolar protein sorting-associated proteins (VPSs) are associated with the endosomal sorting complex required for transport (ESCRT) that plays a role in transporting lipids from the early endosome to Golgi via the multivesicular body pathway (MVP) (114, 115). Their extracellular binding to GSLs mediates their clustering on cells, which is sensed by proteins within the lipid rafts to trigger endocytosis in clathrin-dependent and independent manners (116). GSL trafficking from the plasma membrane to the Golgi network is assisted by a retromer protein complex, which contains different VPS and SNARE proteins of the Syntaxin family. For example, various VPS proteins (such as VPS4A, VPS4B, VPS18, VPS36, and GAPVD1) participate in the retromer complex-mediated sphingolipid translocation from the membrane to the endosome. Categorically, VPS4 and VPS4A are required for retromer complex formation, and VPS4B plays a role

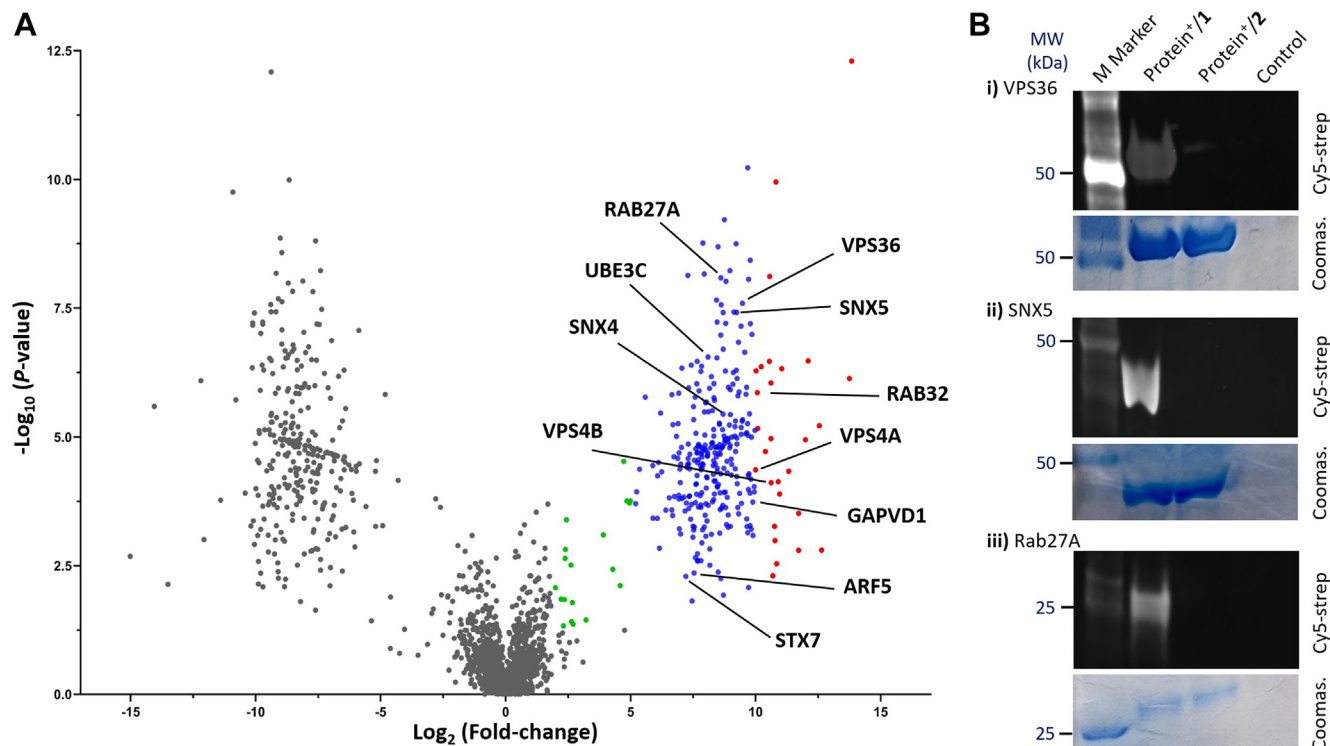


Fig. 5. A: Volcano plot showing the distribution of proteins identified with **1**, presented in \log_2 FC and \log_{10} P, using proteins pulled down by **2** as controls. Color dots indicate significantly ($P < 0.05$) enriched proteins by ≥ 10 (red), 5 (blue), and 2 (green) folds. Some GSL-related proteins reported in the literature are specially marked. B: Cy5-streptavidin blot (top of each panel) and corresponding Coomassie staining (bottom of each panel) images of anti-FLAG resin-isolated proteins from i) FLAG-VPS36, ii) FLAG-SNX5, and iii) FLAG-Rab27A overexpressing HEK293 cells incubated with **1** (protein⁺/1) and **2** (protein⁺/2) or from wild-type cells (control) after UV light-mediated protein crosslinking and then biotinylation via a click reaction, to validate the specific interaction between **1** and VPS36, SNX5, or Rab27A proteins. The whole gel images are presented in [supplemental Fig. S16](#).

in ESCRT-III complex disassembly in an ATP-driven manner. VPS18 and VPS36 contain a ubiquitin-binding domain, regulating membrane trafficking of ubiquitinated proteins via ESCRT-II complex formation (117). VPS18 and VPS36 association with ubiquitinated molecules also supports the presence of ubiquitin ligases or related components (e.g., UBE3C, UCHL3, IRF2BPL, [supplemental Table S1](#)) as unique proteins pulled down by **1**. Syntaxin 7 (STX7), as well as other syntaxin family proteins such as STX5, STX6, and STX16, are engaged in protein or lipid trafficking from plasma membrane to early endosome or other endocytic organelles, thus STX7 is expected to be involved in cellular translocation of GSLs. Sorting nexin proteins 4 and 5 (SNX4 and SNX5) are membrane proteins from the nexin protein family, possessing lipid-binding domains. Other nexins like SNX1 and SNX2 are reported to be present in the retromer complex and required for efficient retrograde transport of GSLs from early endosome to trans-Golgi network. Although there is no report directly linking SNX4 and SNX5 to GSLs, we anticipate that they are also involved in regulating GSL trafficking, because they share a similar sequence as SNX1 and SNX2. Ras-related proteins Rab-27A and Rab-32 are small GTPases, which act as binary on/off

switches to control signal transduction. Other Rab proteins (such as Rab-7 and Rab-9) are known to be important mediators of the Golgi transport and trafficking of caveolae-internalized GSLs (87). Therefore, Rab-27A and Rab-32 are expected to participate in GSL trafficking as well. PALS2 is a protein localized at the lateral membrane of HEK293 cells as a component of mLin-7 complex, which regulates GSL and GPI endocytosis (106).

We also analyzed the unique proteins identified with **2** and attempted to associate them with GSL-related processes but failed to find obvious correlations. This may be due to the unique structure of **2** with a GlcNAc residue directly linked to Cer. This linkage form has not been discovered in mammalian GSLs. Therefore, **2** may not have specific binding targets in the cell.

To further profile the unique proteins identified with **1**, we conducted bioinformatics studies. Gene ontology analysis of the 238 proteins observed in all three experiments indicates that the highly enriched proteins are related to protein and lipid trafficking, endocytosis, and transport ([Fig. 6A](#)). This is not surprising because the first step for GSL participation in various signaling pathways starts with extracellular ligand binding and then endocytosis and redistribution

TABLE 1. GSL-related unique proteins identified with probe 1

Proteins	Uniprot ID	Literature Reported Functions and Associations with GSLs	Ref.
Q9UN37 O75351 Q9P253 Q86VN1 Q14C86 O95219 Q9Y5X3	VPS4A VPS4B VPS18 VPS36 GAPVD1 SNX4 SNX5	Vacuolar protein sorting (VPS) associated proteins, which are known to promote early endosome to Golgi transport of cellular proteins and lipids. GSL-binding Shiga toxins (STXs) requires retromer complex (SNX1 and SNX2, VPS) in their translocation process from cell membrane to trans-Golgi network. Sorting nexin proteins, which possess lipid binding domains. Various SNX proteins along with VPS proteins are key components of the mammalian retromer complex, which regulates GSL transport from endosome to trans-Golgi network.	(79–83) (82–86)
P51159 Q13637	RAB27A RAB32	Rab proteins, which constitute the largest family of small GTPases that regulate cellular protein and lipid transport along the different stages of endocytic pathway. Rabs play an important role in GSL transport from late endosome to trans-Golgi network.	(87–93)
Q8N6T3	ARFGAP1	A GTP-ase activating protein for ADP-ribosylation factor 1, which mediates COPI vesicle formation from Golgi membrane. Binding of ARFGAP1 to the GSL fatty acid chain initiates the membrane bending, which acts as a starting point for different signaling pathway.	(94–96)
Q68EM7	ARHGAP17	A Rho-GTPase activating protein, which participates in Ca ²⁺ -dependent regulation of endocytosis and exocytosis of membrane proteins and glycolipids.	(97–100)
P84085	ARF5	An ADP-ribosylation factor GTPase, which regulates vesicle trafficking. ARF5 regulates the biosynthesis of clathrin-independent endocytosis (CLIC) at the plasma membrane, required for GSL assembly with other signaling molecules.	(101–103)
Q15386	UBE3C	A ubiquitin-protein ligase, which interacts with a particular GSL called N5, to regulate the endocytosis of different notch receptors present on the cell surface. Ubiquitin-protein ligases act as mediators for the interaction between notch receptor and GSLs.	(104, 105)
Q9NZW5	PALS2	A scaffolding protein localized at the lateral membrane of kidney cells. As a component of mLin-7 complex, it interacts with GSLs or GPI anchors to regulate the endocytosis of transmembrane proteins.	(106, 107)
O15400	STX7	A protein from the membrane integrated SNARE protein family. It interacts with GPI-anchored proteins and GSLs to mediate protein trafficking to early endosome.	(108–110)
P84095	RHOG	A Rho-related GTP-binding protein, which interacts with glycolipid transfer proteins to regulate GSL distribution in different intracellular membranes.	(111, 112)
Q13823	GNL2	A nucleolar GTP-binding protein, which acts as GTPase involved in GSL biosynthesis.	(113)

to ER, Golgi, and endosomes. Our analysis of the cellular functions of the unique proteins (Fig. 6B) results in similar conclusions. Functional analysis further reveals proteins that are associated with cytoskeletal rearrangement, cell adhesion, and ATP binding, which is also expected since GSLs are believed to initiate signaling processes via conspicuous cytoskeletal rearrangements (118–120). The remaining proteins are associated with RNA processing and RNA splicing, which is likely caused by probe incorporation into the cytoplasm and nucleus membranes.

Validation of the proteomic results

To verify the proteomic results and prove that the interactions of 1 with the unique proteins pulled down by 1 were specific, we selected three of these proteins, VPS36, SNX5, and Rab27A, as models to perform further in-depth investigation. VPS36 was reported to assist ESCRT in regulating the retrograde transport of multivesicular endosomal (MVE) cargos (121). However, there is no report of direct interactions between VPS36 and GSLs, although GSLs have been found to play a critical role in MVE formation (122–124). SNX5 is

mainly involved in intracellular protein trafficking via the retromer complex by facilitating cargo retrieval from the endosome to the trans-Golgi network. Although SNX proteins often possess GSL-binding domains (82–86), there is no report of GSL binding to SNX5 yet. Rab27A is a membrane-bound protein as an essential component of the melanosome receptor potentially involved in protein, GSL, and small GTPase-mediated signal transduction (125). Here, we aimed to validate that the observed interactions between 1 and VPS36, SNX5, or Rab27A were specific.

In these experiments, first, we overexpressed the target proteins carrying a DYKDDDDK (FLAG) tag using HEK293 cells and commercially available plasmids by established protocols. Next, the cells were incubated with 1 and 2 to label proteins interacting with them, following the procedure described above. Subsequently, the labeled proteins were extracted and applied to the click reaction to introduce a biotin tag. Finally, the target proteins were isolated using anti-FLAG resins and subjected to SDS-PAGE analysis by streptavidin-Cy5 blot. If the target protein is labeled with 1 or 2, it should exhibit Cy5 fluorescence signals;

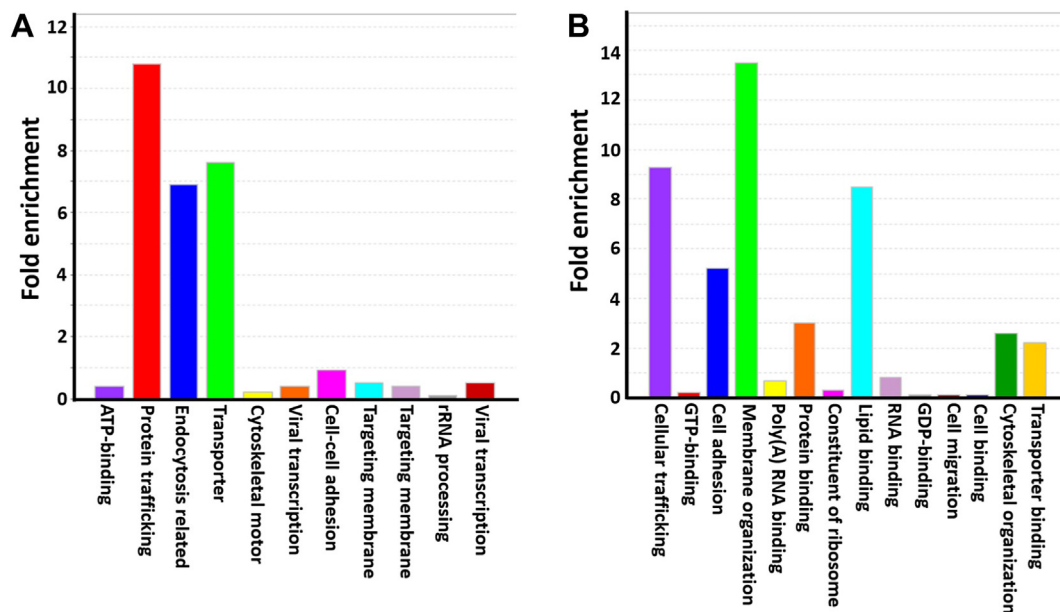


Fig. 6. Gene ontology analysis of the 312 unique proteins pulled down by **1** with respect to (A) biological processes and (B) biological functions. The Y axis shows the folds of enrichment of specific proteins pulled down by probe **1**.

otherwise, the target protein is not labeled with the probe. Our results from protein-overexpressing cells (Fig. 5B and supplemental Fig. S16) clearly indicate that VPS36, SNX5, and Rab27A were labeled by **1** but not by **2**, although cells treated with **1** and **2** expressed the same levels of FLAG-tagged VPS36, SNX5, and Rab27A proteins (see Coomassie blue staining results presented in Fig. 5B and supplemental Fig. S16). These results prove that VPS36, SNX5, and Rab27A crosslinked with **1** specifically, which is in accordance with our proteomic results. Considering that **1** and **2** contain the same lipid moiety and are different only in the glycans, these results are especially interesting, as they demonstrate the great influence of glycans of GSLs on their interaction with cell membranes and biomolecules on cells.

DISCUSSION

To facilitate the investigation of GSL-interacting membrane proteins, we have designed and synthesized bifunctional GSL probes **1** and **2**, which contain photoreactive diazirine and clickable alkyne. This design enables the cross-coupling of probes **1** and **2** with target membrane proteins upon UV irradiation and the labeling of crosslinked proteins with an affinity tag by click reaction to facilitate their isolation and identification, respectively. The design to have the diazirine and alkyne moieties separately located in the lipid and glycan can enhance the specificity of the probes because even if they are metabolically incorporated by cells into other GSLs and biomolecules, the two functional groups are unlikely to be present in the same biosynthetic products to act as bifunctional probes. We anticipate this probe design, as well


as the relevant protocols, to be widely applicable to various GSLs. Eventually, we employed different techniques to validate that both probes **1** and **2** were effectively incorporated into the plasma and intracellular organelle membranes and pulled down specific proteins.

Using **1**, we have identified a series of unique proteins, many of which were previously reported as being related to GSL biosynthesis, trafficking, recycling, cytoskeletal rearrangement, and signaling. Triplicate experiments gave similar results, suggesting the reliability and reproducibility of the method. In addition, we have conducted experiments to further verify that VPS36, SNX5, and Rab27A, which are among the unique proteins pulled down by **1**, indeed interact with **1** specifically. Direct interactions of VPS36, SNX5, and Rab27A with GSLs have not been reported previously. Therefore, we have demonstrated that **1** and **2** are useful probes for studying GSL-membrane interaction and revealing new GSL-binding proteins. Moreover, although the embryonic kidney cell line HEK293 was used for the current work, the method and protocols described here should also be useful for studying other cell lines.

Another discovery of this research is that **1** and **2**, which have the same lipid moiety but different glycans, crosslink to different sets of membrane proteins. This directly proves the decisive influence of the glycan structure of GSLs on their properties or behaviors on the cell surface and their interaction with cellular membranes. It will also be interesting to study if probe **1** and the similar bifunctional derivative of LcGg4, which are epimers differing only in the stereochemistry of one carbon atom (Figs. 1 and 2), bind

to the same membrane proteins or not. We further anticipate that the lipid tail of GSLs can also significantly affect the properties of GSLs and their interaction with membranes, which is another topic of our future research. This problem can be studied using similar GSL probes with different lipid moieties. While disclosing GSL-binding proteins in the plasma membrane is the key to understanding the functional roles and mechanisms of GSLs, identifying GSL-interacting proteins in intracellular membranes is also important, especially for in-depth investigation of the processes related to GSL biosynthesis, metabolism, cellular trafficking, and recycling. In this regard, the proteomic dataset generated herein is useful, although more accurate results can be obtained by modifying the experimental conditions, such as the duration of cellular treatment with the probe, because this can affect the probe distribution within cells. Therefore, the GSL probes developed here can be employed to study these problems as well. Finally, another future direction of this project is to study the identified proteins using techniques like genetic engineering to reveal their functions in GSL-regulated biological and pathological processes.

Data availability

The datasets presented in this study can be found in [Supplemental data](#) of this paper and online repositories. The names of the repositories and the accession number(s) are as follows. The proteomic raw data and search results have been deposited to the ProteomeXchange Consortium via the PRIDE partner repository with the data set identifier PXD030528. 

Supplemental data

This article contains [supplemental data](#) (89, 106, 113, 126–349).

Acknowledgments

ZG is also grateful to Drs Steven and Rebecca Scott for their endowment to support our research.

Author contributions

R. R., S. C., C. L., Z. G., and S. K. writing–review & editing; R. R., S. C., C. L., Z. G., and S. K. writing–original draft; R. R., S. C., S. B., and S. K. validation; R. R., S. C., C. L., Z. G., and S. K. methodology; R. R., S. C., Z. G., and S. K. investigation; R. R., S. C., C. L., S. K. formal analysis; R. R., S. C., C. L., and S. K. data curation; R. R., Z. G., and S. K. conceptualization; S. C., Z. G. resources; Z. G. supervision; Z. G. project administration; Z. G. funding acquisition.

Author ORCIDs

Sayan Kundu  <https://orcid.org/0000-0003-0628-6698>
Rajendra Rohokale  <https://orcid.org/0000-0001-8083-0466>
Chuwei Lin  <https://orcid.org/0000-0002-8640-5695>
Sixue Chen  <https://orcid.org/0000-0002-6690-7612>
Zhongwu Guo  <https://orcid.org/0000-0001-5302-6456>

Funding and additional information

This work is partially supported by an NIH grant (R35 GM131686).

Conflict of interest

The authors declare no conflict of interest.

Abbreviations

AcOH, acetic acid; AGC, automatic gain control; AP, alkaline phosphatase; ATCC, American Type Culture Collection; BCA, bicinchoninic acid; BCIP, 5-bromo-4-chloro-3-indolyl phosphate; BF, bright-field; Boc, *N*-tert-butylloxycarbonyl; BSA, bovine serum albumin; CAA, chloroacetamide; Cer, ceramide; CLIC, clathrin-independent endocytosis; CuAAC, copper-catalyzed alkyne-azide cycloaddition; DAPI, 4',6-diamidino-2-phenylindole; DBU, 1,8-diazabicyclo[5.4.0]undec-7-ene; DCM, dichloromethane; DMAP, 4-dimethylaminopyridine; DMEM, Dulbecco's modified Eagle's medium; DMSO, dimethyl sulfoxide; DPBS, Dulbecco's phosphate buffer saline; DTT, dithiothreitol; EDC, 1-ethyl-3-(3-dimethylaminopropyl)carbodiimide; ER, endoplasmic reticulum; ESCRT, endosomal sorting complex required for transport; EtOAc, ethyl acetate; FA, formic acid; FACS, flow cytometry; FBS, fetal bovine serum; FDR, false discovery rate; FLAG, DYKDDDDK peptide; GalNAc, *N*-acetyl-D-galactosamine; GlcNAc, β -*N*-acetyl-D-glucosamine; GSL, glycosphingolipid; HEK, human embryonic kidney; LC, liquid chromatography; MS, mass spectrometry; MS 4 Å, molecular sieves 4 Å; MVE, multivesicular endosomal; MVP, multivesicular body pathway; NBT, nitro blue tetrazolium; PFA, paraformaldehyde; SDS-PAGE, sodium dodecyl sulfate–polyacrylamide gel electrophoresis; rt, room temperature; SNX, sorting nexin proteins; Strep, streptavidin; STX, syntaxin; TCEP, tris(2-carboxyethyl) phosphine hydrochloride; TFA, trifluoroacetic acid; THPTA, tris(3-hydroxypropyl)triazolylmethylamine; TLC, thin layer chromatography; TMSOTf, trimethylsilyl triflate; Troc, *N*-2,2,2-trichloroethoxycarbonyl; VPS, vacuolar protein sorting-associated protein; WCL, whole cell lysate.

Manuscript received March 19, 2024, and in revised form May 3, 2024. Published, JLR Papers in Press, May 23, 2024, <https://doi.org/10.1016/j.jlr.2024.100570>

REFERENCES

1. Hakomori, S. I. (2008) Structure and function of glycosphingolipids and sphingolipids, recollections and future trends. *Biochim. Biophys. Acta.* **1780**, 325–346
2. Bollinger, C. R., Teichgräber, V., and Gulbins, E. (2005) Ceramide-enriched membrane domains. *Biochim. Biophys. Acta.* **1746**, 284–294
3. Mishra, S., and Joshi, P. G. (2007) Lipid raft heterogeneity: an enigma. *J. Neurochem.* **103 Suppl 1**, 135–142
4. Iwabuchi, K. (2015) Involvement of glycosphingolipid-enriched lipid rafts in inflammatory responses. *Front. Biosci.* **20**, 325–334
5. Nakayama, H., Nagafuku, M., Suzuki, A., Iwabuchi, K., and Inokuchi, J. I. (2018) The regulatory roles of glycosphingolipid-enriched lipid rafts in immune systems. *FEBS Lett.* **592**, 3921–3942
6. Thompson, T. E., and Tillack, T. W. (1985) Organization of glycosphingolipids in bilayers and plasma membranes of mammalian cells. *Annu. Rev. Biophys. Biophys. Chem.* **14**, 361–386

7. D'Angelo, G., Capasso, S., Sticco, L., and Russo, D. (2013) Glycosphingolipids: synthesis and functions. *FEBS J.* **280**, 6338–6353
8. Wennekens, T., van den Berg, R. J., Boot, R. G., van der Marel, G. A., Overkleeft, H. S., and Aerts, J. M. (2009) Glycosphingolipids—nature, function, and pharmacological modulation. *Angew. Chem. Int. Ed. Engl.* **48**, 8848–8869
9. Russo, D., Parashuraman, S., and D'Angelo, G. (2016) Glycosphingolipid-protein interaction in signal transduction. *Int. J. Mol. Sci.* **17**, e1732
10. Ferreira, L., Villar, E., and Muñoz-Barroso, I. (2004) Gangliosides and N-glycoproteins function as Newcastle disease virus receptors. *Int. J. Biochem. Cell Biol.* **36**, 2344–2356
11. Mahfoud, R., Garmy, N., Maresca, M., Yahy, N., Puigserver, A., and Fantini, J. (2002) Identification of a common sphingolipid-binding domain in Alzheimer, prion, and HIV-1 proteins. *J. Biol. Chem.* **277**, 11292–11296
12. Fantini, J., and Yahy, N. (2011) Molecular basis for the glycosphingolipid-binding specificity of α -synuclein: key role of tyrosine 39 in membrane insertion. *J. Mol. Biol.* **408**, 654–669
13. Azzaz, F., Yahy, N., Di Scala, C., Chahinian, H., and Fantini, J. (2022) Ganglioside binding domains in proteins: physiological and pathological mechanisms. *Adv. Protein Chem. Struct. Biol.* **128**, 289–324
14. Hakomori, S. I. (2000) Cell adhesion/recognition and signal transduction through glycosphingolipid microdomain. *Glycoconj. J.* **17**, 143–151
15. Qamsari, E. S., Nourazarian, A., Bagheri, S., and Motallebnezhad, M. (2016) Ganglioside as a therapy target in various types of cancer. *Asian Pac. J. Cancer Prev.* **17**, 1643–1647
16. Groux-Degroote, S., Guerardel, Y., and Delannoy, P. (2017) Gangliosides: structures, biosynthesis, analysis, and roles in cancer. *ChemBioChem.* **18**, 1146–1154
17. Russo, D., L., C., Loomba, J. S., Sticco, L., and D'Angelo, G. (2018) Glycosphingolipid metabolism in cell fate specification. *J. Cell Sci.* **131**, jcs219204
18. Merzak, A., Koochekpour, S., McCrea, S., Roxanis, Y., and Pilkington, G. J. (1995) Gangliosides modulate proliferation, migration, and invasiveness of human brain tumor cells in vitro. *Mol. Chem. Neuropathol.* **24**, 121–135
19. Svennerholm, L. (1994) Gangliosides—a new therapeutic agent against stroke and Alzheimer's disease. *Life Sci.* **55**, 2125–2134
20. Mutoh, T., Hirabayashi, Y., Mihara, T., Ueda, M., Koga, H., Ueda, A., et al. (2006) Role of glycosphingolipids and therapeutic perspectives on Alzheimer's disease. *CNS Neurol. Disord. Drug Targets.* **5**, 375–380
21. Noel, A., Ingrand, S., and Barrier, L. (2017) Ganglioside and related-sphingolipid profiles are altered in a cellular model of Alzheimer's disease. *Biochimie.* **137**, 158–164
22. Memon, R. A., Holleran, W. M., Uchida, Y., Moser, A. H., Grunfeld, C., and Feingold, K. R. (2001) Regulation of sphingolipid and glycosphingolipid metabolism in extrahepatic tissues by endotoxin. *J. Lipid Res.* **42**, 452–459
23. Viard, M., Parolini, I., Rawat, S. S., Fecchi, K., Sargiacomo, M., Puri, A., et al. (2004) The role of glycosphingolipids in HIV signaling, entry and pathogenesis. *Glycoconj. J.* **20**, 213–222
24. Hanada, K. (2005) Sphingolipids in infectious diseases. *Jpn. J. Infect. Dis.* **58**, 131–148
25. Guo, Z. (2022) The structural diversity of natural glycosphingolipids (GSLs). *J. Carbohydr. Chem.* **41**, 63–154
26. Shigeta, K., Ito, Y., Ogawa, T., Kirihata, Y., Hakomori, S., and Kannagi, R. (1987) Monoclonal antibodies directed to chemically synthesized lactogangliotetraosylceramide, a leukemia-associated antigen having a novel branching structure. *J. Biol. Chem.* **262**, 1358–1362
27. Maccioni, H. J., Quiroga, R., and Ferrari, M. L. (2011) Cellular and molecular biology of glycosphingolipid glycosylation. *J. Neurochem.* **117**, 589–602
28. Trotter, J., Klein, C., and Kramer, E. (2000) GPI-anchored proteins and glycosphingolipid-rich rafts: platforms for adhesion and signaling. *Neuroscientist.* **6**, 271–284
29. Tsui-Pierchala, B. A., Encinas, M., Milbrandt, J., and Johnson, E. M., Jr. (2002) Lipid rafts in neuronal signaling and function. *Trends Neurosci.* **25**, 412–417
30. Aureli, M., Grassi, S., Prioni, S., Sonnino, S., and Prinetti, A. (2015) Lipid membrane domains in the brain. *Biochim. Biophys. Acta.* **1851**, 1006–1016
31. Komatsuya, K., Kikuchi, N., Hirabayashi, T., and Kasahara, K. (2023) The regulatory roles of cerebellar glycosphingolipid microdomains/lipid rafts. *Int. J. Mol. Sci.* **24**, 5566
32. Caputto, R., de Maccioni, A. H., and Caputto, B. L. (1977) Studies on the functions of gangliosides in the central nervous system. *Adv. Exp. Med. Biol.* **83**, 289–295
33. Gallego, O., Betts, M. J., Gvozdenovic-Jeremic, J., Maeda, K., Matetzi, C., Aguilar-Gurrieri, C., et al. (2010) A systematic screen for protein-lipid interactions in *Saccharomyces cerevisiae*. *Mol. Syst. Biol.* **6**, 430
34. Zhu, H., Bilgin, M., Bangham, R., Hall, D., Casamayor, A., Bertone, P., et al. (2001) Global analysis of protein activities using proteome chips. *Science.* **293**, 2101–2105
35. Kota, V., Szulc, Z. M., and Hama, H. (2012) Identification of C(6)-ceramide-interacting proteins in D6P2T Schwannoma cells. *Proteomics.* **12**, 2179–2184
36. Bidlingmaier, S., Ha, K., Lee, N. K., Su, Y., and Liu, B. (2016) Proteome-wide identification of novel ceramide-binding proteins by yeast surface cDNA display and deep sequencing. *Mol. Cell. Proteomics.* **15**, 1232–1245
37. Han, L., Kitov, P. I., Li, J., Kitova, E. N., and Klassen, J. S. (2020) Probing heteromultivalent protein-glycosphingolipid interactions using native mass spectrometry and nanodiscs. *Anal. Chem.* **92**, 3923–3931
38. Han, L., Nguyen, L., Schmidt, E. N., Esmaili, M., Kitova, E. N., Overduin, M., et al. (2022) How choice of model membrane affects protein-glycosphingolipid interactions: insights from native mass spectrometry. *Anal. Chem.* **94**, 16042–16049
39. Ideo, H., Seko, A., Ishizuka, I., and Yamashita, K. (2003) The N-terminal carbohydrate recognition domain of galectin-8 recognizes specific glycosphingolipids with high affinity. *Glycobiology.* **13**, 713–723
40. Chakrabandhu, K., Huault, S., Garmy, N., Fantini, J., Stebe, E., Maifert, S., et al. (2008) The extracellular glycosphingolipid-binding motif of Fas defines its internalization route, mode and outcome of signals upon activation by ligand. *Cell Death Differ.* **15**, 1824–1837
41. Heuss, S. F., Tarantino, N., Fantini, J., Ndiaye-Lobry, D., Moretti, J., Israël, A., et al. (2013) A glycosphingolipid binding domain controls trafficking and activity of the mammalian notch ligand delta-like 1. *PLoS One.* **8**, e74392
42. Prasanna, X., Jafurulla, M., Sengupta, D., and Chattopadhyay, A. (2016) The ganglioside GMI interacts with the serotonin(1A) receptor via the sphingolipid binding domain. *Biochim. Biophys. Acta.* **1858**, 2818–2826
43. Tagami, S., Inokuchi, J., Kabayama, K., Yoshimura, H., Kitamura, F., Uemura, S., et al. (2002) Ganglioside GM3 participates in the pathological conditions of insulin resistance. *J. Biol. Chem.* **277**, 3085–3092
44. Coskun, Ü., Grzybek, M., Drechsel, D., and Simons, K. (2011) Regulation of human EGF receptor by lipids. *Proc. Natl. Acad. Sci. U. S. A.* **108**, 9044–9048
45. Park, S. Y., Kwak, C. Y., Shayman, J. A., and Kim, J. H. (2012) Globoside promotes activation of ERK by interaction with the epidermal growth factor receptor. *Biochim. Biophys. Acta.* **1820**, 1141–1148
46. Meuillet, E., Cremel, G., Dreyfus, H., and Hicks, D. (1996) Differential modulation of basic fibroblast and epidermal growth factor receptor activation by ganglioside GM3 in cultured retinal Müller glia. *Glia.* **17**, 206–216
47. Toledo, M. S., Suzuki, E., Handa, K., and Hakomori, S. (2005) Effect of ganglioside and tetraspanins in microdomains on interaction of integrins with fibroblast growth factor receptor. *J. Biol. Chem.* **280**, 16227–16234
48. Mutoh, T., Tokuda, A., Miyadai, T., Hamaguchi, M., and Fujiki, N. (1995) Ganglioside GMI binds to the Trk protein and regulates receptor function. *Proc. Natl. Acad. Sci. U. S. A.* **92**, 5087–5091
49. Rabin, S. J., and Mocchetti, I. (1995) GMI ganglioside activates the high-affinity nerve growth factor receptor trkA. *J. Neurochem.* **65**, 347–354
50. Cazet, A., Lefebvre, J., Adriaenssens, E., Julien, S., Bobowski, M., Grigoriadis, A., et al. (2010) GD₃ synthase expression enhances proliferation and tumor growth of MDA-MB-231 breast cancer cells through c-Met activation. *Mol. Cancer Res.* **8**, 1526–1535

51. Yates, A. J., Saqr, H. E., and Van Brocklyn, J. (1995) Ganglioside modulation of the PDGF receptor. A model for ganglioside functions. *J. Neurooncol.* **24**, 65–73
52. Chung, T. W., Kim, S. J., Choi, H. J., Kim, K. J., Kim, M. J., Kim, S. H., *et al.* (2009) Ganglioside GM3 inhibits VEGF/VEGFR-2-mediated angiogenesis: direct interaction of GM3 with VEGFR-2. *Glycobiology*. **19**, 229–239
53. Ge, J., Du, S., and Yao, S. Q. (2022) Bifunctional lipid-derived affinity-based probes (AfBPs) for analysis of lipid-protein interactome. *Acc. Chem. Res.* **55**, 3663–3674
54. Peng, T., Yuan, X., and Hang, H. C. (2014) Turning the spotlight on protein-lipid interactions in cells. *Curr. Opin. Chem. Biol.* **21**, 144–153
55. Haberkant, P., and Holthuis, J. C. (2014) Fat & fabulous: bifunctional lipids in the spotlight. *Biochim. Biophys. Acta.* **1841**, 1022–1030
56. Niphakis, M. J., Lum, K. M., Coggnetta 3rd, A. B., Correia, B. E., Ichu, T. A., Olucha, J., *et al.* (2015) A global map of lipid-binding proteins and their ligandability in cells. *Cell*. **161**, 1668–1680
57. Haberkant, P., Rajmakers, R., Wildwater, M., Sachsenheimer, T., Brügger, B., Maeda, K., *et al.* (2013) In vivo profiling and visualization of cellular protein-lipid interactions using bifunctional fatty acids. *Angew. Chem. Int. Ed. Engl.* **52**, 4033–4038
58. Hulce, J. J., Coggnetta, A. B., Niphakis, M. J., Tully, S. E., and Cravatt, B. F. (2013) Proteome-wide mapping of cholesterol-interacting proteins in mammalian cells. *Nat. Methods*. **10**, 259–264
59. Höglinger, D., Nadler, A., Haberkant, P., Kirkpatrick, J., Schifferer, M., Stein, F., *et al.* (2017) Trifunctional lipid probes for comprehensive studies of single lipid species in living cells. *Proc. Natl. Acad. Sci. U. S. A.* **114**, 1566–1571
60. Kundu, S., Lin, C., Jaiswal, M., Mullapudi, V. B., Craig, K. C., Chen, S., *et al.* (2023) Profiling glycosylphosphatidylinositol (GPI)-interacting proteins in the cell membrane using a bifunctional GPI analogue as the probe. *J. Proteome Res.* **22**, 919–930
61. Kundu, S., Jaiswal, M., Babu Mullapudi, V., Guo, J., Kamat, M., Basso, K. B., *et al.* (2024) Investigation of glycosylphosphatidylinositol (GPI)-plasma membrane interaction in live cells and the influence of GPI glycan structure on the interaction. *Chem. Eur. J.* **30**, e202303047
62. Das, J. (2011) Aliphatic diazirines as photoaffinity probes for proteins: recent development. *Chem. Rev.* **111**, 4405–4417
63. Smith, E., and Collins, I. (2015) Photoaffinity labeling in target- and binding-site identification. *Future Med. Chem.* **7**, 159–183
64. Murale, D. P., Hong, S. C., Haque, M. M., and Lee, J. S. (2016) Photo-affinity labeling (PAL) in chemical proteomics: a handy tool to investigate protein-protein interactions (PPIs). *Proteome Sci.* **15**, 14
65. Komura, K., Yamazaki, A., Imamura, A., Ishida, H., Kiso, M., and Ando, H. (2017) Syntheses of bifunctional photoaffinity ganglioside probes for studying fast-associated interactions. *Trends Carbohydr. Res.* **9**, 1–26
66. Yu, W., and Baskin, J. M. (2022) Photoaffinity labeling approaches to elucidate lipid-protein interactions. *Curr. Opin. Chem. Biol.* **69**, 102173
67. Mullapudi, V. B., Craig, K. C., and Guo, Z. (2022) Design and synthesis of a doubly functionalized core structure of a glycosylphosphatidylinositol anchor containing photoreactive and clickable functional groups. *J. Org. Chem.* **87**, 9419–9425
68. Wang, D., Du, S., Cazenave-Gassiot, A., Ge, J., Lee, J. S., Wenk, M. R., *et al.* (2017) Global mapping of protein-lipid interactions by using modified choline-containing phospholipids metabolically synthesized in live cells. *Angew. Chem. Int. Ed.* **56**, 5829–5833
69. Rohokale, R. S., Li, Q., and Guo, Z. (2021) A diversity-oriented strategy for chemical synthesis of glycosphingolipids: synthesis of glycosphingolipid LcGg4 and its analogues and derivatives. *J. Org. Chem.* **86**, 1633–1648
70. Thomas, P., and Smart, T. G. (2005) HEK293 cell line: a vehicle for the expression of recombinant proteins. *J. Pharmacol. Toxicol. Methods.* **51**, 187–200
71. Geiger, T., Wehner, A., Schaab, C., Cox, J., and Mann, M. (2012) Comparative proteomic analysis of eleven common cell lines reveals ubiquitous but varying expression of most proteins. *Mol. Cell. Proteomics.* **11**, M111.014050
72. Lavado-García, J., Jorge, I., Cervera, L., Vázquez, J., and Gòdia, F. (2020) Multiplexed quantitative proteomic analysis of HEK293 provides insights into molecular changes associated with the cell density effect, transient transfection, and virus-like particle production. *J. Proteome Res.* **19**, 1085–1099
73. Huang, Y. F., Aoki, K., Akase, S., Ishihara, M., Liu, Y. S., Yang, G., *et al.* (2021) Global mapping of glycosylation pathways in human-derived cells. *Dev. Cell*. **56**, 1195–1209.e7
74. Paulick, M. G., Forstner, M. B., Groves, J. T., and Bertozzi, C. R. (2007) A chemical approach to unraveling the biological function of the glycosylphosphatidylinositol anchor. *PNAS.* **104**, 20332–20337
75. van Meer, G., and Lisman, Q. (2002) Sphingolipid transport: rafts and translocators. *J. Biol. Chem.* **277**, 25855–25858
76. Silence, D. J. (2007) New insights into glycosphingolipid functions-storage, lipid rafts, and translocators. *Int. Rev. Cytol.* **262**, 151–189
77. Arai, K., Kanie, Y., Kanie, O., Fukase, K., and Kabayama, K. (2020) Temporal analysis of localization and trafficking of glycolipids. *Biochem. Biophys. Res. Commun.* **532**, 19–24
78. Halter, D., Neumann, S., van Dijk, S. M., Wolthoorn, J., de Mazière, A. M., Vieira, O. V., *et al.* (2007) Pre- and post-Golgi translocation of glucosylceramide in glycosphingolipid synthesis. *J. Cell Biol.* **179**, 101–115
79. Ewers, H., and Helenius, A. (2011) Lipid-mediated endocytosis. *Cold Spring Harb. Perspect. Biol.* **3**, a004721
80. Hurley, J. H., and Emr, S. D. (2006) The ESCRT complexes: structure and mechanism of a membrane-trafficking network. *Annu. Rev. Biophys. Biomol. Struct.* **35**, 277–298
81. Katzmann, D. J., Odorizzi, G., and Emr, S. D. (2002) Receptor downregulation and multivesicular-body sorting. *Nat. Rev. Mol. Cell Biol.* **3**, 893–905
82. Bonifacino, J. S., and Hurley, J. H. (2008) Retromer. *Curr. Opin. Cell Biol.* **20**, 427–436
83. Attar, N., and Cullen, P. J. (2010) The retromer complex. *Adv. Enzyme Regul.* **50**, 216–236
84. Dyve, A. B., Bergan, J., Utskarpen, A., and Sandvig, K. (2009) Sorting nexin 8 regulates endosome-to-Golgi transport. *Biochem. Biophys. Res. Commun.* **390**, 109–114
85. Rangarajan, E. S., Park, H., Fortin, E., Sygusch, J., and Izard, T. (2010) Mechanism of aldolase control of sorting nexin 9 function in endocytosis. *J. Biol. Chem.* **285**, 11983–11990
86. Johannes, L., Parton, R. G., Bassereau, P., and Mayor, S. (2015) Building endocytic pits without clathrin. *Nat. Rev. Mol. Cell Biol.* **16**, 311–321
87. Choudhury, A., Dominguez, M., Puri, V., Sharma, D. K., Narita, K., Wheatley, C. L., *et al.* (2002) Rab proteins mediate Golgi transport of caveola-internalized glycosphingolipids and correct lipid trafficking in Niemann-Pick C cells. *J. Clin. Invest.* **109**, 1541–1550
88. Seaman, M. N., Harbour, M. E., Tattersall, D., Read, E., and Bright, N. (2009) Membrane recruitment of the cargo-selective retromer subcomplex is catalysed by the small GTPase Rab7 and inhibited by the Rab-GAP TBC1D5. *J. Cell Sci.* **122**, 2371–2382
89. Marks, D. L., and Pagano, R. E. (2002) Endocytosis and sorting of glycosphingolipids in sphingolipid storage disease. *Trends Cell Biol.* **12**, 605–613
90. Binnington, B., Nguyen, L., Kamani, M., Hossain, D., Marks, D. L., Budani, M., *et al.* (2016) Inhibition of Rab prenylation by statins induces cellular glycosphingolipid remodeling. *Glycobiology.* **26**, 166–180
91. Silence, D. J., and Platt, F. M. (2004) Glycosphingolipids in endocytic membrane transport. *Semin. Cell Dev. Biol.* **15**, 409–416
92. Stein, M. P., Dong, J., and Wandinger-Ness, A. (2003) Rab proteins and endocytic trafficking: potential targets for therapeutic intervention. *Adv. Drug Deliv. Rev.* **55**, 1421–1437
93. Rojas, R., van Vlijmen, T., Mardones, G. A., Prabhu, Y., Rojas, A. L., Mohammed, S., *et al.* (2008) Regulation of retromer recruitment to endosomes by sequential action of Rab5 and Rab7. *J. Cell Biol.* **183**, 513–526
94. Kitamata, M., Inaba, T., and Suetsugu, S. (2020) The roles of the diversity of amphipathic lipids in shaping membranes by membrane-shaping proteins. *Biochem. Soc. Trans.* **48**, 837–851
95. Doherty, G. J., Åhnlund, M. K., Howes, M. T., Morén, B., Parton, R. G., McMahon, H. T., *et al.* (2011) The endocytic protein GRAF1 is directed to cell-matrix adhesion sites and regulates cell spreading. *Mol. Biol. Cell.* **22**, 4380–4389

96. Fernández-Ulbarri, I., Vilella, M., Lázaro-Diéguez, F., Sarri, E., Martínez, S. E., Jiménez, N., *et al.* (2007) Diacylglycerol is required for the formation of COPI vesicles in the Golgi-to-ER transport pathway. *Mol. Biol. Cell* **18**, 3250–3263
97. Richnau, N., and Aspenström, P. (2001) Rich, a rho GTPase-activating protein domain-containing protein involved in signaling by Cdc42 and Rac1. *J. Biol. Chem.* **276**, 35060–35070
98. Ellis, S., and Mellor, H. (2000) Regulation of endocytic traffic by rho family GTPases. *Trends Cell Biol.* **10**, 85–88
99. Wesén, E., Lundmark, R., and Esbjörner, E. K. (2020) Role of membrane tension sensitive endocytosis and rho GTPases in the uptake of the Alzheimer's disease peptide $\alpha\beta(1-42)$. *ACS Chem. Neurosci.* **11**, 1925–1936
100. Kirkham, M., and Parton, R. G. (2005) Clathrin-independent endocytosis: new insights into caveolae and non-caveolar lipid raft carriers. *Biochim. Biophys. Acta.* **1745**, 273–286
101. Lebsir, N., Goueslain, L., Farhat, R., Callens, N., Dubuisson, J., Jackson, C. L., *et al.* (2019) Functional and physical interaction between the arf activator GBF1 and hepatitis C virus NS3 protein. *J. Virol.* **93**, e01459-18
102. Jackson, C. L., and Bouvet, S. (2014) Arfs at a glance. *J. Cell Sci.* **127**, 4103–4109
103. De Franceschi, N., Hamidi, H., Alanko, J., Sahgal, P., and Ivaska, J. (2015) Integrin traffic - the update. *J. Cell Sci.* **128**, 839–852
104. Hamel, S., Fantini, J., and Schweisguth, F. (2010) Notch ligand activity is modulated by glycosphingolipid membrane composition in *Drosophila melanogaster*. *J. Cell Biol.* **188**, 581–594
105. Cuevas-Navarro, A., Van, R., Cheng, A., Urisman, A., Castel, P., and McCormick, F. (2021) The RAS GTPase RIT1 compromises mitotic fidelity through spindle assembly checkpoint suppression. *Curr. Biol.* **31**, 3915–3924.e9
106. Straight, S. W., Chen, L., Karnak, D., and Margolis, B. (2001) Interaction with mLin-7 alters the targeting of endocytosed transmembrane proteins in mammalian epithelial cells. *Mol. Biol. Cell.* **12**, 1329–1340
107. Kamberov, E., Makarova, O., Roh, M., Liu, A., Karnak, D., Straight, S., *et al.* (2000) Molecular cloning and characterization of Pals, proteins associated with mLin-7. *J. Biol. Chem.* **275**, 11425–11431
108. Kalus, I., Hodel, A., Koch, A., Kleene, R., Edwardson, J. M., and Schrader, M. (2002) Interaction of syncollin with GP-2, the major membrane protein of pancreatic zymogen granules, and association with lipid microdomains. *Biochem. J.* **362**, 433–442
109. Sieber, J. J., Willig, K. I., Heintzmann, R., Hell, S. W., and Lang, T. (2006) The SNARE motif is essential for the formation of syntaxin clusters in the plasma membrane. *Biophys. J.* **90**, 2843–2851
110. Levic, D. S., and Bagnat, M. (2022) Self-organization of apical membrane protein sorting in epithelial cells. *FEBS J.* **289**, 659–670
111. Yang, F., Guan, Y., Feng, X., Rolfs, A., Schlüter, H., and Luo, J. (2019) Proteomics of the corpus callosum to identify novel factors involved in hypomyelinated Niemann-Pick Type C disease mice. *Mol. Brain.* **12**, 17
112. Banerjee, A., Ray, A., Barpanda, A., Dash, A., Gupta, I., Nissa, M. U., *et al.* (2022) Evaluation of autoantibody signatures in pituitary adenoma patients using human proteome arrays. *Proteomics Clin. Appl.* **16**, e2100111
113. Liang, X., Zuo, M. Q., Zhang, Y., Li, N., Ma, C., Dong, M. Q., *et al.* (2020) Structural snapshots of human pre-60S ribosomal particles before and after nuclear export. *Nat. Commun.* **11**, 3542
114. Eden, E. R., Burgoyne, T., Edgar, J. R., Sorkin, A., and Futter, C. E. (2012) The relationship between ER-multivesicular body membrane contacts and the ESCRT machinery. *Biochem. Soc. Trans.* **40**, 464–468
115. Schmidt, O., and Teis, D. (2012) The ESCRT machinery. *Curr. Biol.* **22**, R116–R120
116. Cho, J. A., Chinnapen, D. J-F., Aamar, E., Welscher, Y. M., Lencer, W. I., and Massol, R. (2012) Insights on the trafficking and retro-translocation of glycosphingolipid-binding bacterial toxins. *Front. Cell. Infect. Microbiol.* **2**, 1–6
117. Slagsvold, T., Aasland, R., Hirano, S., Bache, K. G., Raiborg, C., Trambaiolo, D., *et al.* (2005) Eap45 in mammalian ESCRT-II binds ubiquitin via a phosphoinositide-interacting GLUE domain. *J. Biol. Chem.* **280**, 19600–19606
118. Iwabuchi, K., Nakayama, H., Iwahara, C., and Takamori, K. (2010) Significance of glycosphingolipid fatty acid chain length on membrane microdomain-mediated signal transduction. *FEBS Lett.* **584**, 1642–1652
119. Kraft, M. L. (2016) Sphingolipid organization in the plasma membrane and the mechanisms that influence it. *Front. Cell Dev. Biol.* **4**, 154
120. Cumin, C., Huang, Y. L., Everest-Dass, A., and Jacob, F. (2021) Deciphering the importance of glycosphingolipids on cellular and molecular mechanisms associated with epithelial-to-mesenchymal transition in cancer. *Biomolecules.* **11**, 62
121. Babst, M., Katzmann, D. J., Snyder, W. B., Wendland, B., and Emr, S. D. (2002) Endosome-associated complex, ESCRT-II, recruits transport machinery for protein sorting at the multivesicular body. *Dev. Cell.* **3**, 283–289
122. Bieberich, E. (2018) Sphingolipids and lipid rafts: novel concepts and methods of analysis. *Chem. Phys. Lipids.* **216**, 114–131
123. Kufareva, I., Lenoir, M., Dancea, F., Sridhar, P., Raush, E., Bissig, C., *et al.* (2014) Discovery of novel membrane binding structures and functions. *Biochem. Cell Biol.* **92**, 555–563
124. Im, Y. J., and Hurley, J. H. (2008) Integrated structural model and membrane targeting mechanism of the human ESCRT-II complex. *Dev. Cell.* **14**, 902–913
125. Wu, X., Wang, F., Rao, K., Sellers, J. R., and Hammer 3rd, J. A. (2002) Rab27a is an essential component of melanosome receptor for myosin Va. *Mol. Biol. Cell.* **13**, 1735–1749
126. Kim, J. H., Yang, C. K., Heo, K., Roeder, R. G., An, W., and Stallcup, M. R. (2008) CCAR1, a key regulator of mediator complex recruitment to nuclear receptor transcription complexes. *Mol. Cell.* **31**, 510–519
127. Consortium, U. (2021) UniProt: the universal protein knowledgebase in 2021. *Nucleic Acids Res.* **49**, D480–D489
128. Möller, I., Beatrix, B., Kreibich, G., Sakai, H., Lauring, B., and Wiedmann, M. (1998) Unregulated exposure of the ribosomal M-site caused by NAC depletion results in delivery of non-secretory polypeptides to the Sec61 complex. *FEBS Lett.* **441**, 1–5
129. Yotov, W. V., and St-Arnaud, R. (1996) Differential splicing-in of a proline-rich exon converts alphaNAC into a muscle-specific transcription factor. *Genes Dev.* **10**, 1763–1772
130. Kovtun, O., Tillu, V. A., Ariotti, N., Parton, R. G., and Collins, B. M. (2015) Cavin family proteins and the assembly of caveolae. *J. Cell Sci.* **128**, 1269–1278
131. Syrovatkina, V., Alegre, K. O., Dey, R., and Huang, X. Y. (2016) Regulation, signaling, and physiological functions of G-proteins. *J. Mol. Biol.* **428**, 3850–3868
132. Liu, C. C., Liu, Y. Y., Zhou, J. F., Chen, X., Chen, H., Hu, J. H., *et al.* (2022) Cellular ESCRT components are recruited to regulate the endocytic trafficking and RNA replication compartment assembly during classical swine fever virus infection. *PLoS Pathog.* **18**, e1010294
133. Kabe, Y., Goto, M., Shima, D., Imai, T., Wada, T., Morohashi, K., *et al.* (1999) The role of human MBF1 as a transcriptional coactivator. *J. Biol. Chem.* **274**, 34196–34202
134. Prieto-Sánchez, R. M., Berenjano, I. M., and Bustelo, X. R. (2006) Involvement of the Rho/Rac family member RhoG in caveolar endocytosis. *Oncogene.* **25**, 2961–2973
135. Zou, Q., and Qi, H. (2021) Deletion of ribosomal paralogs Rpl39 and Rpl39l compromises cell proliferation via protein synthesis and mitochondrial activity. *Int. J. Biochem. Cell Biol.* **139**, 106070
136. Hubbard, C., Singleton, D., Rauch, M., Jayasinghe, S., Cafiso, D., and Castle, D. (2000) The secretory carrier membrane protein family: structure and membrane topology. *Mol. Biol. Cell.* **11**, 2933–2947
137. Hata, S., Sorimachi, H., Nakagawa, K., Maeda, T., Abe, K., and Suzuki, K. (2001) Domain II of m-calpain is a Ca(2+)-dependent cysteine protease. *FEBS Lett.* **501**, 111–114
138. Merino-Trigo, A., Kerr, M. C., Houghton, F., Lindberg, A., Mitchell, C., Teasdale, R. D., *et al.* (2004) Sorting nexin 5 is localized to a subdomain of the early endosomes and is recruited to the plasma membrane following EGF stimulation. *J. Cell Sci.* **117**, 6413–6424
139. Sampson, J., Richards, M. W., Choi, J., Fry, A. M., and Bayliss, R. (2021) Phase-separated foci of EML4-ALK facilitate signalling and depend upon an active kinase conformation. *EMBO Rep.* **22**, e53693
140. Gustafsson Sheppard, N., Jarl, L., Mahadessian, D., Strittmatter, L., Schmidt, A., Madhusudan, N., *et al.* (2015) The folate-coupled enzyme MTHFD2 is a nuclear protein and promotes cell proliferation. *Sci. Rep.* **5**, 15029

141. Espinha, G., Osaki, J. H., Magalhaes, Y. T., and Forti, F. L. (2015) Rac1 GTPase-deficient HeLa cells present reduced DNA repair, proliferation, and survival under UV or gamma irradiation. *Mol. Cell. Biochem.* **404**, 281–297
142. Illigmann, A., Thoma, Y., Pan, S., Reinhardt, L., and Brötz-Oesterhelt, H. (2021) Contribution of the Clp protease to bacterial survival and mitochondrial homeostasis. *Microb. Physiol.* **31**, 260–279
143. Coelho, A. R., and Oliveira, P. J. (2020) Dihydroorotate dehydrogenase inhibitors in SARS-CoV-2 infection. *Eur. J. Clin. Invest.* **50**, e13366
144. Conti, M. (2000) Phosphodiesterases and cyclic nucleotide signaling in endocrine cells. *Mol. Endocrinol.* **14**, 1317–1327
145. Berger, K., Lindh, R., Wierup, N., Zmuda-Trzebiatowska, E., Lindqvist, A., Manganiello, V. C., et al. (2009) Phosphodiesterase 3B is localized in caveolae and smooth ER in mouse hepatocytes and is important in the regulation of glucose and lipid metabolism. *PLoS One* **4**, e4671
146. Tulin, E. E., Onoda, N., Hasegawa, M., Nosaka, T., Nomura, H., and Kitamura, T. (2002) Genetic approach and phenotype-based complementation screening for identification of stroma cell-derived proteins involved in cell proliferation. *Exp. Cell Res.* **272**, 23–31
147. Donaldson, J. G., and Jackson, C. L. (2011) ARF family G proteins and their regulators: roles in membrane transport, development and disease. *Nat. Rev. Mol. Cell Biol.* **12**, 362–375
148. Sato, M., Sato, K., Fonarev, P., Huang, C. J., Liou, W., and Grant, B. D. (2005) *Caenorhabditis elegans* RME-6 is a novel regulator of RAB-5 at the clathrin-coated pit. *Nat. Cell Biol.* **7**, 559–569
149. Renard, H. F., Tyckaert, F., Lo Giudice, C., Hirsch, T., Valades-Cruz, C. A., Lemaigre, C., et al. (2020) Endophilin-A3 and Galectin-8 control the clathrin-independent endocytosis of CD166. *Nat. Commun.* **11**, 1457
150. Vainberg, I. E., Lewis, S. A., Rommelaere, H., Ampe, C., Vandekerckhove, J., Klein, H. L., et al. (1998) Prefoldin, a chaperone that delivers unfolded proteins to cytosolic chaperonin. *Cell.* **93**, 863–873
151. Cárce1-Trullols, J., Kovács, A. D., and Pearce, D. A. (2015) Cell biology of the NCL proteins: what they do and don't do. *Biochim. Biophys. Acta.* **1852**, 2242–2255
152. Fujisawa, K., Terai, S., Takami, T., Yamamoto, N., Yamasaki, T., Matsumoto, T., et al. (2016) Modulation of anti-cancer drug sensitivity through the regulation of mitochondrial activity by adenylate kinase 4. *J. Exp. Clin. Cancer Res.* **35**, 48
153. Rojas, A. M., Fuentes, G., Rausell, A., and Valencia, A. (2012) The Ras protein superfamily: evolutionary tree and role of conserved amino acids. *J. Cell Biol.* **196**, 189–201
154. Lata, S., Schoehn, G., Jain, A., Pires, R., Piehler, J., Gottlinger, H. G., et al. (2008) Helical structures of ESCRT-III are disassembled by VPS4. *Science.* **321**, 1354–1357
155. Dermody, J. L., and Buratowski, S. (2010) Leo1 subunit of the yeast pafl complex binds RNA and contributes to complex recruitment. *J. Biol. Chem.* **285**, 33671–33679
156. Angrisani, A., Di Fiore, A., De Smaele, E., and Moretti, M. (2021) The emerging role of the KCTD proteins in cancer. *Cell Commun. Signal.* **19**, 56
157. Gundelfinger, E. D., Reissner, C., and Garner, C. C. (2015) Role of bassoon and piccolo in assembly and molecular organization of the active zone. *Front. Synaptic Neurosci.* **7**, 19
158. Magaña-Acosta, M., and Valadez-Graham, V. (2020) Chromatin remodelers in the 3D nuclear compartment. *Front. Genet.* **11**, 600615
159. Zhan, X., Yan, C., Zhang, X., Lei, J., and Shi, Y. (2018) Structure of a human catalytic step I spliceosome. *Science.* **359**, 537–545
160. Cai, M., Li, H., Chen, R., and Zhou, X. (2021) MRPL13 Promotes tumor cell proliferation, migration and EMT process in breast cancer through the PI3K-AKT-mTOR pathway. *Cancer Manag. Res.* **13**, 2009–2024
161. Esposti, M. D. (2002) The roles of Bid. *Apoptosis.* **7**, 433–440
162. Takagi, M., Sueishi, M., Saiwaki, T., Kametaka, A., and Yoneda, Y. (2001) A novel nucleolar protein, NIFK, interacts with the forkhead associated domain of Ki-67 antigen in mitosis. *J. Biol. Chem.* **276**, 25386–25391
163. Li, H., Byeon, I. J., Ju, Y., and Tsai, M. D. (2004) Structure of human Ki67 FHA domain and its binding to a phosphoprotein fragment from hNIFK reveal unique recognition sites and new views to the structural basis of FHA domain functions. *J. Mol. Biol.* **335**, 371–381
164. Schapira, M., Tyers, M., Torrent, M., and Arrowsmith, C. H. (2017) WD40 repeat domain proteins: a novel target class? *Nat. Rev. Drug Discov.* **16**, 773–786
165. Fraga de Andrade, I., Mehta, C., and Bresnick, E. H. (2020) Post-transcriptional control of cellular differentiation by the RNA exosome complex. *Nucleic Acids Res.* **48**, 11913–11928
166. Ramalho-Oliveira, R., Oliveira-Vieira, B., and Viola, J. P. B. (2019) IRF2BP2: a new player in the regulation of cell homeostasis. *J. Leukoc. Biol.* **106**, 717–723
167. Xu, F., Du, W., Zou, Q., Wang, Y., Zhang, X., Xing, X., et al. (2021) COPII mitigates ER stress by promoting formation of ER whorls. *Cell Res.* **31**, 141–156
168. Rao, J., Wu, X., Zhou, X., Deng, R., and Ma, Y. (2020) TMEM205 is an independent prognostic factor and is associated with immune cell infiltrates in hepatocellular carcinoma. *Front. Genet.* **11**, 575776
169. Abella, J. V., Galloni, C., Pernier, J., Barry, D. J., Kjær, S., Carlier, M. F., et al. (2016) Isoform diversity in the Arp2/3 complex determines actin filament dynamics. *Nat. Cell Biol.* **18**, 76–86
170. Takahashi, M., and Kobayashi, T. (2009) Cholesterol regulation of rab-mediated sphingolipid endocytosis. *Glycoconj. J.* **26**, 705–710
171. D'Souza-Schorey, C., and Chavrier, P. (2006) ARF proteins: roles in membrane traffic and beyond. *Nat. Rev. Mol. Cell Biol.* **7**, 347–358
172. Geldner, N. (2004) The plant endosomal system—its structure and role in signal transduction and plant development. *Planta.* **219**, 547–560
173. Sívá, M., Svoboda, M., Veverka, V., Trempe, J. F., Hofmann, K., Kožíšek, M., et al. (2016) Human DNA-damage-inducible 2 protein is structurally and functionally distinct from its yeast ortholog. *Sci. Rep.* **6**, 30443
174. Huang, S., Dong, X., Wang, J., Ding, J., Li, Y., Li, D., et al. (2018) Overexpression of the ubiquilin-4 (UBQLN4) is associated with cell cycle arrest and apoptosis in human normal gastric epithelial cell lines GES-1 cells by activation of the ERK signaling pathway. *Med. Sci. Monit.* **24**, 3564–3570
175. Lee, J. H., Jomaa, A., Chung, S., Hwang Fu, Y. H., Qian, R., Sun, X., et al. (2021) Receptor compaction and GTPase rearrangement drive SRP-mediated cotranslational protein translocation into the ER. *Sci. Adv.* **7**, eabg0942
176. Levine, A. J. (1997) p53, the cellular gatekeeper for growth and division. *Cell.* **88**, 323–331
177. Samper-Martín, B., Sarrías, A., Lázaro, B., Pérez-Montero, M., Rodríguez-Rodríguez, R., Ribeiro, M. P. C., et al. (2021) Polyphosphate degradation by Nudt3-Zn. *Cell Rep.* **37**, 110004
178. Kavanagh, K. L., Jörnvall, H., Persson, B., and Oppermann, U. (2008) Medium- and short-chain dehydrogenase/reductase gene and protein families: the SDR superfamily: functional and structural diversity within a family of metabolic and regulatory enzymes. *Cell. Mol. Life Sci.* **65**, 3895–3906
179. Maeda, Y., Tanaka, S., Hino, J., Kangawa, K., and Kinoshita, T. (2000) Human dolichol-phosphate-mannose synthase consists of three subunits, DPML, DPM2 and DPM3. *EMBO J.* **19**, 2475–2482
180. Timchenko, N. A., Cai, Z. J., Welm, A. L., Reddy, S., Ashizawa, T., and Timchenko, L. T. (2001) RNA CUG repeats sequester CUGBP1 and alter protein levels and activity of CUGBP1. *J. Biol. Chem.* **276**, 7820–7826
181. Rochman, M., Malicet, C., and Bustin, M. (2010) HMG5/NSBPI: a new member of the HMG protein family that affects chromatin structure and function. *Biochim. Biophys. Acta.* **1799**, 86–92
182. Jin, S. B., Zhao, J., Bjork, P., Schmekel, K., Ljungdahl, P. O., and Wieslander, L. (2002) Mrd1p is required for processing of pre-rRNA and for maintenance of steady-state levels of 40 S ribosomal subunits in yeast. *J. Biol. Chem.* **277**, 18431–18439
183. Snider, J., Kittanakom, S., Damjanovic, D., Curak, J., Wong, V., and Stagljar, I. (2010) Detecting interactions with membrane proteins using a membrane two-hybrid assay in yeast. *Nat. Protoc.* **5**, 1281–1293
184. Russo, L. C., Farias, J. O., Ferruzo, P. Y. M., Monteiro, L. F., and Forti, F. L. (2018) Revisiting the roles of VHR/DUSP3 phosphatase in human diseases. *Clinics (Sao Paulo).* **73**, e466s

185. Wendeler, M. W., Paccaud, J. P., and Hauri, H. P. (2007) Role of Sec24 isoforms in selective export of membrane proteins from the endoplasmic reticulum. *EMBO Rep.* **8**, 258–264
186. Akiyama, H., Fujisawa, N., Tashiro, Y., Takanabe, N., Sugiyama, A., and Tashiro, F. (2003) The role of transcriptional corepressor Nif3l1 in early stage of neural differentiation via cooperation with Trip15/CSN2. *J. Biol. Chem.* **278**, 10752–10762
187. Lu, X., Ng, H. H., and Bubulya, P. A. (2014) The role of SON in splicing, development, and disease. *Wiley Interdiscip. Rev. RNA.* **5**, 637–646
188. Hu, H., Wang, Z., Li, M., Zeng, F., Wang, K., Huang, R., et al. (2017) Gene expression and methylation analyses suggest DCTD as a prognostic factor in malignant glioma. *Sci. Rep.* **7**, 11568
189. Schou, K. B., Mogensen, J. B., Morthorst, S. K., Nielsen, B. S., Aleliunaite, A., Serra-Marques, A., et al. (2017) KIF13B establishes a CAV1-enriched microdomain at the ciliary transition zone to promote Sonic hedgehog signalling. *Nat. Commun.* **8**, 14177
190. Rachlin, A. S., and Otey, C. A. (2006) Identification of palladin isoforms and characterization of an isoform-specific interaction between Lasp-1 and palladin. *J. Cell Sci.* **119**, 995–1004
191. Bend, R., Cohen, L., Carter, M. T., Lyons, M. J., Niyazov, D., Mikati, M. A., et al. (2020) Phenotype and mutation expansion of the PTPN23 associated disorder characterized by neurodevelopmental delay and structural brain abnormalities. *Eur. J. Hum. Genet.* **28**, 76–87
192. Tanabe, K., Kon, S., Ichijo, N., Funaki, T., Natsume, W., Watanabe, T., et al. (2008) A SMAP gene family encoding ARF GTPase-activating proteins and its implication in membrane trafficking. *Methods Enzymol.* **438**, 155–170
193. Brobeil, A., Bobrich, M., Tag, C., and Wimmer, M. (2012) PTPIP51 in protein interactions: regulation and in situ interacting partners. *Cell Biochem. Biophys.* **63**, 211–222
194. Tu, Y., Popov, S., Slaughter, C., and Ross, E. M. (1999) Palmitoylation of a conserved cysteine in the regulator of G protein signaling (RGS) domain modulates the GTPase-activating activity of RGS4 and RGS10. *J. Biol. Chem.* **274**, 38260–38267
195. Schwarz, R. I. (2015) Collagen I and the fibroblast: high protein expression requires a new paradigm of post-transcriptional, feedback regulation. *Biochem. Biophys. Rep.* **3**, 38–44
196. Kapoor, N., Gupta, R., Menon, S. T., Folta-Stogniew, E., Raleigh, D. P., and Sakmar, T. P. (2010) Nucleobindin 1 is a calcium-regulated guanine nucleotide dissociation inhibitor of G α 1 β . *J. Biol. Chem.* **285**, 31647–31660
197. Kevenaar, J. T., Bianchi, S., van Spronsen, M., Olieric, N., Lipka, J., Frias, C. P., et al. (2016) Kinesin-binding protein controls microtubule dynamics and cargo trafficking by regulating kinesin motor activity. *Curr. Biol.* **26**, 849–861
198. Herlihy, A. E., Boeing, S., Weems, J. C., Walker, J., Dirac-Svejstrup, A. B., Lehner, M. H., et al. (2022) UBAP2/UBAP2L regulate UV-induced ubiquitylation of RNA polymerase II and are the human orthologues of yeast Def1. *DNA Repair (Amst)*. **115**, 103343
199. Cavdar Koc, E., Burkhart, W., Blackburn, K., Moseley, A., and Spremulli, L. L. (2001) The small subunit of the mammalian mitochondrial ribosome. Identification of the full complement of ribosomal proteins present. *J. Biol. Chem.* **276**, 19363–19374
200. Burns, R., Majczenko, K., Xu, J., Peng, W., Yapici, Z., Dowling, J. J., et al. (2014) Homozygous splice mutation in CWF19L1 in a Turkish family with recessive ataxia syndrome. *Neurology*. **83**, 2175–2182
201. Rosing, M., Ossendorf, E., Rak, A., and Barnekow, A. (2007) Giantin interacts with both the small GTPase Rab6 and Rab1. *Exp. Cell Res.* **313**, 2318–2325
202. Guo, X., Engel, J. L., Xiao, J., Tagliabracci, V. S., Wang, X., Huang, L., et al. (2011) UBLCP1 is a 26S proteasome phosphatase that regulates nuclear proteasome activity. *Proc. Natl. Acad. Sci. U. S. A.* **108**, 18649–18654
203. Boczonadi, V., Müller, J. S., Pyle, A., Munkley, J., Dor, T., Quarataro, J., et al. (2014) EXOSC8 mutations alter mRNA metabolism and cause hypomyelination with spinal muscular atrophy and cerebellar hypoplasia. *Nat. Commun.* **5**, 4287
204. Sbrissa, D., Ikonov, O. C., Fu, Z., Ijuin, T., Gruenberg, J., Takenawa, T., et al. (2007) Core protein machinery for mammalian phosphatidylinositol 3,5-bisphosphate synthesis and turnover that regulates the progression of endosomal transport. Novel Sac phosphatase joins the ArPIKfyve-PIKfyve complex. *J. Biol. Chem.* **282**, 23878–23891
205. Goppelt, A., Stelzer, G., Lottspeich, F., and Meisterernst, M. (1996) A mechanism for repression of class II gene transcription through specific binding of NC2 to TBP-promoter complexes via heterodimeric histone fold domains. *EMBO J.* **15**, 3105–3116
206. Damianov, A., Kann, M., Lane, W. S., and Bindereif, A. (2006) Human RBM28 protein is a specific nucleolar component of the spliceosomal snRNPs. *Biol. Chem.* **387**, 1455–1460
207. Ye, Y., Shibata, Y., Yun, C., Ron, D., and Rapoport, T. A. (2004) A membrane protein complex mediates retro-translocation from the ER lumen into the cytosol. *Nature*. **429**, 841–847
208. Vukotic, M., Oeljeklaus, S., Wiese, S., Vögtle, F. N., Meisinger, C., Meyer, H. E., et al. (2012) Rcf1 mediates cytochrome oxidase assembly and respirasome formation, revealing heterogeneity of the enzyme complex. *Cell. Metab.* **15**, 336–347
209. Huang, G., Shigesada, K., Ito, K., Wee, H. J., Yokomizo, T., and Ito, Y. (2001) Dimerization with PEBP2beta protects RUNX1/AML1 from ubiquitin-proteasome-mediated degradation. *EMBO J.* **20**, 723–733
210. Burman, J. L., Bourbonniere, L., Philie, J., Stroth, T., Dejgaard, S. Y., Presley, J. F., et al. (2008) Scyll1, mutated in a recessive form of spinocerebellar neurodegeneration, regulates COPI-mediated retrograde traffic. *J. Biol. Chem.* **283**, 22774–22786
211. Sarkar, A. A., and Zohn, I. E. (2012) Hectd1 regulates intracellular localization and secretion of Hsp90 to control cellular behavior of the cranial mesenchyme. *J. Cell Biol.* **196**, 789–800
212. Adams, G. N., LaRusch, G. A., Stavrou, E., Zhou, Y., Nieman, M. T., Jacobs, G. H., et al. (2011) Murine prolylcarboxypeptidase depletion induces vascular dysfunction with hypertension and faster arterial thrombosis. *Blood*. **117**, 3929–3937
213. Koc, E. C., Burkhart, W., Blackburn, K., Moyer, M. B., Schlatzer, D. M., Moseley, A., et al. (2001) The large subunit of the mammalian mitochondrial ribosome. Analysis of the complement of ribosomal proteins present. *J. Biol. Chem.* **276**, 43958–43969
214. Agrimi, G., Russo, A., Scarcia, P., and Palmieri, F. (2012) The human gene SLC25A17 encodes a peroxisomal transporter of coenzyme A, FAD and NAD⁺. *Biochem. J.* **443**, 241–247
215. Barik, S., and Banerjee, A. K. (1992) Phosphorylation by cellular casein kinase II is essential for transcriptional activity of vesicular stomatitis virus phosphoprotein P. *Proc. Natl. Acad. Sci. U. S. A.* **89**, 6570–6574
216. Kalousek, F., Isaya, G., and Rosenberg, L. E. (1992) Rat liver mitochondrial intermediate peptidase (MIP): purification and initial characterization. *EMBO J.* **11**, 2803–2809
217. Kondo, H., Matsumura, T., Kaneko, M., Inoue, K., Kosako, H., Ikawa, M., et al. (2020) PITHD1 is a proteasome-interacting protein essential for male fertilization. *J. Biol. Chem.* **295**, 1658–1672
218. Vazquez-Sanchez, S., Gonzalez-Lozano, M. A., Walfenzao, A., Li, K. W., and van Weering, J. R. T. (2020) The endosomal protein sorting nexin 4 is a synaptic protein. *Sci. Rep.* **10**, 18239
219. Teng, F. Y., Wang, Y., and Tang, B. L. (2001) The syntaxins. *Genome Biol.* **2**, REVIEWS3012
220. Ciccarelli, F. D., Proukakis, C., Patel, H., Cross, H., Azam, S., Patton, M. A., et al. (2003) The identification of a conserved domain in both spartin and spastin, mutated in hereditary spastic paraplegia. *Genomics*. **81**, 437–441
221. Vagin, O., Tokhtaeva, E., Garay, P. E., Souda, P., Bassilian, S., Whitelegge, J. P., et al. (2014) Recruitment of septin cytoskeletal proteins by botulinum toxin A protease determines its remarkable stability. *J. Cell Sci.* **127**, 3294–3308
222. Keele, G. R., Prokop, J. W., He, H., Holl, K., Littrell, J., Deal, A. W., et al. (2021) Sept8/SEPTIN8 involvement in cellular structure and kidney damage is identified by genetic mapping and a novel human tubule hypoxic model. *Sci. Rep.* **11**, 2071
223. Fürst, M., Zhou, Y., Merfort, J., and Müller, M. (2018) Involvement of PpiD in sec-dependent protein translocation. *Biochim. Biophys. Acta Mol. Cell Res.* **1865**, 273–280
224. Lahiri, S., Lee, H., Mesicek, J., Fuks, Z., Haimovitz-Friedman, A., Kolesnick, R. N., et al. (2007) Kinetic characterization of mammalian ceramide synthases: determination of K(m) values towards sphinganine. *FEBS Lett.* **581**, 5289–5294

225. McNally, T., Huang, Q., Janis, R. S., Liu, Z., Olejniczak, E. T., and Reilly, R. M. (2003) Structural analysis of UBL5, a novel ubiquitin-like modifier. *Protein Sci.* **12**, 1562–1566
226. Ni, C., Schmitz, D. A., Lee, J., Pawlowski, K., Wu, J., and Buszczak, M. (2022) Labeling of heterochronic ribosomes reveals Clorf109 and SPATA5 control a late step in human ribosome assembly. *Cell Rep.* **38**, 110597
227. Lin, C., Zhang, J., Lu, Y., Li, X., Zhang, W., Lin, W., *et al.* (2018) NIT1 suppresses tumour proliferation by activating the TGF β 1-Smad2/3 signalling pathway in colorectal cancer. *Cell Death Dis.* **9**, 263
228. Kutzleb, C., Sanders, G., Yamamoto, R., Wang, X., Lichte, B., Petrasch-Parwez, E., *et al.* (1998) Paralemmin, a prenyl-palmitoyl-anchored phosphoprotein abundant in neurons and implicated in plasma membrane dynamics and cell process formation. *J. Cell Biol.* **143**, 795–813
229. Jurica, M. S., Licklider, L. J., Gygi, S. R., Grigorieff, N., and Moore, M. J. (2002) Purification and characterization of native spliceosomes suitable for three-dimensional structural analysis. *RNA.* **8**, 426–439
230. Xu, G. F., O'Connell, P., Viskochil, D., Cawthon, R., Robertson, M., Culver, M., *et al.* (1990) The neurofibromatosis type 1 gene encodes a protein related to GAP. *Cell.* **62**, 599–608
231. Dong, H., O'Brien, R. J., Fung, E. T., Lanahan, A. A., Worley, P. F., and Huganir, R. L. (1997) GRIP: a synaptic PDZ domain-containing protein that interacts with AMPA receptors. *Nature.* **386**, 279–284
232. Prendergast, J., Umanah, G. K., Yoo, S. W., Lagerlöf, O., Motari, M. G., Cole, R. N., *et al.* (2014) Ganglioside regulation of AMPA receptor trafficking. *J. Neurosci.* **34**, 13246–13258
233. Cheadle, L., and Biederer, T. (2012) The novel synaptogenic protein Farpl links postsynaptic cytoskeletal dynamics and transsynaptic organization. *J. Cell Biol.* **199**, 985–1001
234. Lin, A., Minden, A., Martinetto, H., Claret, F. X., Lange-Carter, C., Mercurio, F., *et al.* (1995) Identification of a dual specificity kinase that activates the Jun kinases and p38-Mpk2. *Science.* **268**, 286–290
235. Kremer, B. E., Haystead, T., and Macara, I. G. (2005) Mammalian septins regulate microtubule stability through interaction with the microtubule-binding protein MAP4. *Mol. Biol. Cell.* **16**, 4648–4659
236. Meng, G., Zhao, Y., Bai, X., Liu, Y., Green, T. J., Luo, M., *et al.* (2010) Structure of human stabilin-1 interacting chitinase-like protein (SI-CLP) reveals a saccharide-binding cleft with lower sugar-binding selectivity. *J. Biol. Chem.* **285**, 39898–39904
237. McPherson, P. S. (1999) Regulatory role of SH3 domain-mediated protein-protein interactions in synaptic vesicle endocytosis. *Cell. Signal.* **11**, 229–238
238. Poulard, C., Rambaud, J., Hussein, N., Corbo, L., and Le Romancer, M. (2014) JMJD6 regulates ER α methylation on arginine. *PLoS One.* **9**, e87982
239. Wu, W., Chen, Y., Ye, S., Yang, H., Yang, J., and Quan, J. (2021) Transcription factor forkhead box K1 regulates miR-32 expression and enhances cell proliferation in colorectal cancer. *Oncol. Lett.* **21**, 407
240. Sun, N., Critchley, D. R., Paulin, D., Li, Z., and Robson, R. M. (2008) Human alpha-synemin interacts directly with vinculin and metavinculin. *Biochem. J.* **409**, 657–667
241. Tu, C., Ortega-Cava, C. F., Winograd, P., Stanton, M. J., Reddi, A. L., Dodge, L., *et al.* (2010) Endosomal-sorting complexes required for transport (ESCRT) pathway-dependent endosomal traffic regulates the localization of active Src at focal adhesions. *Proc. Natl. Acad. Sci. U. S. A.* **107**, 16107–16112
242. You, K. T., Park, J., and Kim, V. N. (2015) Role of the small subunit processome in the maintenance of pluripotent stem cells. *Genes Dev.* **29**, 2004–2009
243. Raemaekers, T., Ribbeck, K., Beaudouin, J., Annaert, W., Van Camp, M., Stockmans, I., *et al.* (2003) NuSAP, a novel microtubule-associated protein involved in mitotic spindle organization. *J. Cell Biol.* **162**, 1017–1029
244. Carsberg, C. J., Myers, K. A., and Stern, P. L. (1996) Metastasis-associated 5T4 antigen disrupts cell-cell contacts and induces cellular motility in epithelial cells. *Int. J. Cancer.* **68**, 84–92
245. Pastor-Anglada, M., and Pérez-Torras, S. (2018) Emerging roles of nucleoside transporters. *Front. Pharmacol.* **9**, 606
246. Ding, J., Wang, K., Liu, W., She, Y., Sun, Q., Shi, J., *et al.* (2016) Pore-forming activity and structural autoinhibition of the gasdermin family. *Nature.* **535**, 111–116
247. Falck, J., Mailand, N., Syljuåsen, R. G., Bartek, J., and Lukas, J. (2001) The ATM-Chk2-Cdc25A checkpoint pathway guards against radioresistant DNA synthesis. *Nature.* **410**, 842–847
248. Tang, T., Zheng, B., Chen, S. H., Murphy, A. N., Kudlicka, K., Zhou, H., *et al.* (2009) hNOA1 interacts with complex I and DAP3 and regulates mitochondrial respiration and apoptosis. *J. Biol. Chem.* **284**, 5414–5424
249. Yan, B. R., Li, T., Coyaud, E., Laurent, E. M. N., St-Germain, J., Zhou, Y., *et al.* (2022) C5orf51 is a component of the Mon1-CCZ1 complex and controls RAB7A localization and stability during mitophagy. *Autophagy.* **18**, 829–840
250. Lin-Moshier, Y., Sebastian, P. J., Higgins, L., Sampson, N. D., Hewitt, J. E., and Marchant, J. S. (2013) Re-evaluation of the role of calcium homeostasis endoplasmic reticulum protein (CHERP) in cellular calcium signaling. *J. Biol. Chem.* **288**, 355–367
251. Laity, J. H., Lee, B. M., and Wright, P. E. (2001) Zinc finger proteins: new insights into structural and functional diversity. *Curr. Opin. Struct. Biol.* **11**, 39–46
252. Otten, E. G., Werner, E., Crespillo-Casado, A., Boyle, K. B., Dharamdasani, V., Pathe, C., *et al.* (2021) Ubiquitylation of lipopolysaccharide by RNF213 during bacterial infection. *Nature.* **594**, 111–116
253. Hurtado-Lorenzo, A., Skinner, M., El Annan, J., Futai, M., Sun-Wada, G. H., Bourgoin, S., *et al.* (2006) V-ATPase interacts with ARNO and Arf6 in early endosomes and regulates the protein degradative pathway. *Nat. Cell Biol.* **8**, 124–136
254. Collard, F., Delpierre, G., Stroobant, V., Matthijs, G., and Van Schaftingen, E. (2003) A mammalian protein homologous to fructosamine-3-kinase is a ketosamine-3-kinase acting on p-sicosamines and ribulosamines but not on fructosamines. *Diabetes.* **52**, 2888–2895
255. Adulcikas, J., Norouzi, S., Bretag, L., Sohal, S. S., and Myers, S. (2018) The zinc transporter SLC39A7 (ZIP7) harbours a highly-conserved histidine-rich N-terminal region that potentially contributes to zinc homeostasis in the endoplasmic reticulum. *Comput. Biol. Med.* **100**, 196–202
256. Pühringer, T., Hohmann, U., Fin, L., Pacheco-Fiallos, B., Schellhaas, U., Brennecke, J., *et al.* (2020) Structure of the human core transcription-export complex reveals a hub for multivalent interactions. *Elife.* **9**, e61503
257. Kassel, O., Schneider, S., Heilbock, C., Litfin, M., Göttlicher, M., and Herrlich, P. (2004) A nuclear isoform of the focal adhesion LIM-domain protein Trip6 integrates activating and repressing signals at AP-1- and NF-kappaB-regulated promoters. *Genes Dev.* **18**, 2518–2528
258. Yue, Y., Liu, J., Cui, X., Cao, J., Luo, G., Zhang, Z., *et al.* (2018) VIRMA mediates preferential m6A mRNA methylation in 3'UTR and near stop codon and associates with alternative polyadenylation. *Cell Discov.* **4**, 10
259. Yoshimoto, R., Okawa, K., Yoshida, M., Ohno, M., and Kataoka, N. (2014) Identification of a novel component C2ORF3 in the lariat-intron complex: lack of C2ORF3 interferes with pre-mRNA splicing via intron turnover pathway. *Genes Cells.* **19**, 78–87
260. Sato, O., Sakai, T., Choo, Y. Y., Ikebe, R., Watanabe, T. M., and Ikebe, M. (2022) Mitochondria-associated myosin 19 processively transports mitochondria on actin tracks in living cells. *J. Biol. Chem.* **298**, 101883
261. Saito, Y., Nakagawa, T., Kakihana, A., Nakamura, Y., Nabika, T., Kasai, M., *et al.* (2016) Yeast two-hybrid and one-hybrid screenings identify regulators of hsp70 gene expression. *J. Cell. Biochem.* **117**, 2109–2117
262. Kwiatkowski, S., Seliga, A. K., Vertommen, D., Terreri, M., Ishikawa, T., Grabowska, I., *et al.* (2018) SETD3 protein is the actin-specific histidine N-methyltransferase. *Elife.* **7**, e37921
263. Firestein, R., and Cleary, M. L. (2001) Pseudo-phosphatase Sbf1 contains an N-terminal GEF homology domain that modulates its growth regulatory properties. *J. Cell Sci.* **114**, 2921–2927
264. Caron, C., Pivot-Pajot, C., van Grunsven, L. A., Col, E., Lestrat, C., Rousseaux, S., *et al.* (2003) Cdy1: a new transcriptional corepressor. *EMBO Rep.* **4**, 877–882

265. Wu, K., He, J., Pu, W., and Peng, Y. (2018) The role of exportin-5 in microRNA biogenesis and cancer. *Genomics Proteomics Bioinformatics*. **16**, 120–126
266. Gallo, L. I., Liao, Y., Ruiz, W. G., Clayton, D. R., Li, M., Liu, Y. J., et al. (2014) TBC1D9B functions as a GTPase-activating protein for Rab11a in polarized MDCK cells. *Mol. Biol. Cell*. **25**, 3779–3797
267. Bajaj, L., Sharma, J., di Ronza, A., Zhang, P., Eblimit, A., Pal, R., et al. (2020) A CLN6-CLN8 complex recruits lysosomal enzymes at the ER for Golgi transfer. *J. Clin. Invest.* **130**, 4118–4132
268. Brdicka, T., Pavlistová, D., Leo, A., Bruyns, E., Korínek, V., Angelisová, P., et al. (2000) Phosphoprotein associated with glycosphingolipid-enriched microdomains (PAG), a novel ubiquitously expressed transmembrane adaptor protein, binds the protein tyrosine kinase csk and is involved in regulation of T cell activation. *J. Exp. Med.* **191**, 1591–1604
269. Ohtake, H., Ichikawa, N., Okada, M., and Yamashita, T. (2002) Cutting edge: transmembrane phosphoprotein Csk-binding protein/phosphoprotein associated with glycosphingolipid-enriched microdomains as a negative feedback regulator of mast cell signaling through the FcεRI. *J. Immunol.* **168**, 2087–2090
270. Smida, M., Posevitz-Fejfar, A., Horejsi, V., Schraven, B., and Lindquist, J. A. (2007) A novel negative regulatory function of the phosphoprotein associated with glycosphingolipid-enriched microdomains: blocking Ras activation. *Blood*. **110**, 596–615
271. Svec, A. (2008) Phosphoprotein associated with glycosphingolipid-enriched microdomains/Csk-binding protein: a protein that matters. *Pathol. Res. Pract.* **204**, 785–792
272. Yu, W., Wang, Y., Gong, M., Pei, F., and Zheng, J. (2012) Phosphoprotein associated with glycosphingolipid microdomains I inhibits the proliferation and invasion of human prostate cancer cells in vitro through suppression of Ras activation. *Oncol. Rep.* **28**, 606–614
273. Lizarbe, M. A., Barrasa, J. I., Olmo, N., Gavilanes, F., and Turnay, J. (2013) Annexin-phospholipid interactions. Functional implications. *Int. J. Mol. Sci.* **14**, 2652–2683
274. Burns, A. L., Magendzo, K., Shirvan, A., Srivastava, M., Rojas, E., Aljani, M. R., et al. (1989) Calcium channel activity of purified human synexin and structure of the human synexin gene. *Proc. Natl. Acad. Sci. U. S. A.* **86**, 3798–3802
275. Sheriff, A., Gaip, U. S., Franz, S., Heyder, P., Voll, R. E., Kalden, J. R., et al. (2004) Loss of GM1 surface expression precedes annexin V-phycoerythrin binding of neutrophils undergoing spontaneous apoptosis during in vitro aging. *Cytometry A*. **62**, 75–80
276. Benz, J., and Hofmann, A. (1997) Annexins: from structure to function. *Biol. Chem.* **378**, 177–183
277. Sharom, F. J. (2014) Complex interplay between the P-glycoprotein multidrug efflux pump and the membrane: its role in modulating protein function. *Front. Oncol.* **4**, 41
278. Neumann, J., Rose-Sperling, D., and Hellmich, U. A. (2017) Diverse relations between ABC transporters and lipids: an overview. *Biochim. Biophys. Acta Biomembr.* **1859**, 605–618
279. Tarling, E. J., de Aguiar Vallim, T. Q., and Edwards, P. A. (2013) Role of ABC transporters in lipid transport and human disease. *Trends Endocrinol. Metab.* **24**, 342–350
280. Quazi, F., and Molday, R. S. (2013) Differential phospholipid substrates and directional transport by ATP-binding cassette proteins ABCA1, ABCA7, and ABCA4 and disease-causing mutants. *J. Biol. Chem.* **288**, 34414–34426
281. Wu, A., Wojtowicz, K., Savary, S., Hamon, Y., and Trombik, T. (2020) Do ABC transporters regulate plasma membrane organization? *Cell. Mol. Biol. Lett.* **25**, 37
282. Bigay, J., and Antony, B. (2012) Curvature, lipid packing, and electrostatics of membrane organelles: defining cellular territories in determining specificity. *Dev. Cell*. **23**, 886–895
283. Zerial, M., and McBride, H. (2001) Rab proteins as membrane organizers. *Nat. Rev. Mol. Cell Biol.* **2**, 107–117
284. Pagano, R. E., Martin, O. C., Kang, H. C., and Haugland, R. P. (1991) A novel fluorescent ceramide analogue for studying membrane traffic in animal cells: accumulation at the Golgi apparatus results in altered spectral properties of the sphingolipid precursor. *J. Cell Biol.* **113**, 1267–1279
285. Bremer, E. G., Hakomori, S., Bowen-Pope, D. F., Raines, E., and Ross, R. (1984) Ganglioside-mediated modulation of cell growth, growth factor binding, and receptor phosphorylation. *J. Biol. Chem.* **259**, 6818–6825
286. Cevher-Keskin, B. (2013) ARF1 and SARI GTPases in endomembrane trafficking in plants. *Int. J. Mol. Sci.* **14**, 18181–18199
287. Zhang, N., and Zabolina, O. A. (2022) Critical determinants in ER-Golgi trafficking of enzymes involved in glycosylation. *Plants*. **11**, 428
288. Zoldoš, V., Grgurević, S., and Lauc, G. (2010) Epigenetic regulation of protein glycosylation. *Biomol. Concepts*. **1**, 253–261
289. Masone, M. C., Morra, V., and Venditti, R. (2019) Illuminating the membrane contact sites between the endoplasmic reticulum and the trans-Golgi network. *FEBS Lett.* **593**, 3135–3148
290. Wright, K. J., Baye, L. M., Olivier-Mason, A., Mukhopadhyay, S., Sang, L., Kwong, M., et al. (2011) An ARL3-UNC119-RP2 GTPase cycle targets myristoylated NPHP3 to the primary cilium. *Genes Dev.* **25**, 2347–2360
291. Shumar, S. A., Kerr, E. W., Geldenhuys, W. J., Montgomery, G. E., Fagone, P., Thirawatananond, P., et al. (2018) Nudt19 is a renal CoA diphosphohydrolase with biochemical and regulatory properties that are distinct from the hepatic Nudt7 isoform. *J. Biol. Chem.* **293**, 4134–4148
292. Hatsuzawa, K., and Sakurai, C. (2020) Regulatory mechanism of SNAP23 in phagosome formation and maturation. *Yonago Acta Med.* **63**, 135–145
293. Zhang, Y., Zhang, X. F., Fleming, M. R., Amiri, A., El-Hassar, L., Surguchev, A. A., et al. (2016) Kv3.3 channels bind Hax-1 and Arp2/3 to assemble a stable local actin network that regulates channel gating. *Cell*. **165**, 434–448
294. Pons-Vizcarra, M., Kurps, J., Tawfik, B., Sørensen, J. B., van Weering, J. R. T., and Verhage, M. (2019) MUNC18-1 regulates the submembrane F-actin network, independently of syntaxin1 targeting, via hydrophobicity in β -sheet 10. *J. Cell Sci.* **132**, jcs234674
295. Kaneko, T., Hamazaki, J., Iemura, S., Sasaki, K., Furuyama, K., Natsume, T., et al. (2009) Assembly pathway of the mammalian proteasome base subcomplex is mediated by multiple specific chaperones. *Cell*. **137**, 914–925
296. Wen, Y., and Shatkin, A. J. (1999) Transcription elongation factor hSPT5 stimulates mRNA capping. *Genes Dev.* **13**, 1774–1779
297. Zhang, Y., Zhao, M., Gao, H., Yu, G., Zhao, Y., Yao, F., et al. (2022) MAPK signalling-induced phosphorylation and subcellular translocation of PDH1 α promotes tumour immune evasion. *Nat. Metab.* **4**, 374–388
298. Falcon, A., Doege, H., Fluitt, A., Tsang, B., Watson, N., Kay, M. A., et al. (2010) FATP2 is a hepatic fatty acid transporter and peroxisomal very long-chain acyl-CoA synthetase. *Am. J. Physiol. Endocrinol. Metab.* **299**, E384–E393
299. Conrotto, P., Corso, S., Gamberini, S., Comoglio, P. M., and Giordano, S. (2004) Interplay between scatter factor receptors and B plexins controls invasive growth. *Oncogene*. **23**, 5131–5137
300. Holzmann, J., Frank, P., Löffler, E., Bennett, K. L., Gerner, C., and Rossmannith, W. (2008) RNase P without RNA: identification and functional reconstitution of the human mitochondrial tRNA processing enzyme. *Cell*. **135**, 462–474
301. Makarova, O. V., Makarov, E. M., and Lührmann, R. (2001) The 65 and 110 kDa SR-related proteins of the U4/U6.U5 tri-snRNP are essential for the assembly of mature spliceosomes. *EMBO J.* **20**, 2553–2563
302. Gradi, A., Imataka, H., Svitkin, Y. V., Rom, E., Raught, B., Morino, S., et al. (1998) A novel functional human eukaryotic translation initiation factor 4G. *Mol. Cell. Biol.* **18**, 334–342
303. Bartke, T., Pohl, C., Pyrowolakis, G., and Jentsch, S. (2004) Dual role of BRUCE as an antiapoptotic IAP and a chimeric E2/E3 ubiquitin ligase. *Mol. Cell*. **14**, 801–811
304. Zhang, W., Wang, L., Liu, Y., Xu, J., Zhu, G., Cang, H., et al. (2009) Structure of human lanthionine synthetase C-like protein 1 and its interaction with Eps8 and glutathione. *Genes Dev.* **23**, 1387–1392
305. Chen, S., Blank, M. F., Iyer, A., Huang, B., Wang, L., Grummt, I., et al. (2016) SIRT7-dependent deacetylation of the U3-55k protein controls pre-rRNA processing. *Nat. Commun.* **7**, 10734
306. Leary, S. C., Kaufman, B. A., Pellicchia, G., Guercin, G. H., Mattman, A., Jaksch, M., et al. (2004) Human SCO1 and SCO2

- have independent, cooperative functions in copper delivery to cytochrome c oxidase. *Hum. Mol. Genet.* **13**, 1839–1848
307. Ruyrberg, C., Hajibagheri, M. A., Parry, D. A., and Watt, F. M. (1997) Periplakin, a novel component of cornified envelopes and desmosomes that belongs to the plakin family and forms complexes with envoplakin. *J. Cell Biol.* **139**, 1835–1849
 308. Ohkuni, A., Ohno, Y., and Kihara, A. (2013) Identification of acyl-CoA synthetases involved in the mammalian sphingosine 1-phosphate metabolic pathway. *Biochem. Biophys. Res. Commun.* **442**, 195–201
 309. Maki, T., Grimaldi, A. D., Fuchigami, S., Kaverina, I., and Hayashi, I. (2015) CLASP2 has two distinct TOG domains that contribute differently to microtubule dynamics. *J. Mol. Biol.* **427**, 2379–2395
 310. Sanchez, M. I., Mercer, T. R., Davies, S. M., Shearwood, A. M., Nygård, K. K., Richman, T. R., et al. (2011) RNA processing in human mitochondria. *Cell Cycle* **10**, 2904–2916
 311. Fransen, M., Terlecky, S. R., and Subramani, S. (1998) Identification of a human PTS1 receptor docking protein directly required for peroxisomal protein import. *Proc. Natl. Acad. Sci. U. S. A.* **95**, 8087–8092
 312. Bracken, A. P., Pasini, D., Capra, M., Prosperini, E., Colli, E., and Helin, K. (2003) EZH2 is downstream of the pRB-E2F pathway, essential for proliferation and amplified in cancer. *EMBO J.* **22**, 5323–5335
 313. Ito, T., Yang, M., and May, W. S. (1999) RAX, a cellular activator for double-stranded RNA-dependent protein kinase during stress signaling. *J. Biol. Chem.* **274**, 15427–15432
 314. Hirano, T., Kishi, M., Sugimoto, H., Taguchi, R., Obinata, H., Ohshima, N., et al. (2009) Thioesterase activity and subcellular localization of acylprotein thioesterase 1/lysophospholipase 1. *Biochim. Biophys. Acta.* **1791**, 797–805
 315. Stroud, D. A., Surgenor, E. E., Formosa, L. E., Reljic, B., Frazier, A. E., Dibley, M. G., et al. (2016) Accessory subunits are integral for assembly and function of human mitochondrial complex I. *Nature.* **538**, 123–126
 316. Marteiijn, J. A., van der Meer, L. T., van Emst, L., van Reijmersdal, S., Wissink, W., de Witte, T., et al. (2007) Gfi1 ubiquitination and proteasomal degradation is inhibited by the ubiquitin ligase Triad1. *Blood.* **110**, 3128–3135
 317. Itakura, E., Kishi-Itakura, C., and Mizushima, N. (2012) The hairpin-type tail-anchored SNARE syntaxin 17 targets to autophagosomes for fusion with endosomes/lysosomes. *Cell.* **151**, 1256–1269
 318. Rauch, J. N., Zuiderweg, E. R., and Gestwicki, J. E. (2016) Non-canonical interactions between heat shock cognate protein 70 (Hsc70) and Bcl2-associated anthanogene (BAG) co-chaperones are important for client release. *J. Biol. Chem.* **291**, 19848–19857
 319. Liu, Y. S., Guo, X. Y., Hirata, T., Rong, Y., Motooka, D., Kitajima, T., et al. (2018) Glycan-dependent protein folding and endoplasmic reticulum retention regulate GPI-anchor processing. *J. Cell Biol.* **217**, 585–599
 320. Kalousek, F., Darigo, M. D., and Rosenberg, L. E. (1980) Isolation and characterization of propionyl-CoA carboxylase from normal human liver. Evidence for a protomeric tetramer of nonidentical subunits. *J. Biol. Chem.* **255**, 60–65
 321. Nag, S., Ma, Q., Wang, H., Chumnarnsilpa, S., Lee, W. L., Larsson, M., et al. (2009) Ca²⁺ binding by domain 2 plays a critical role in the activation and stabilization of gelsolin. *Proc. Natl. Acad. Sci. U. S. A.* **106**, 13713–13718
 322. Hunt, T. W., Fields, T. A., Casey, P. J., and Peralta, E. G. (1996) RGS10 is a selective activator of G α i GTPase activity. *Nature.* **383**, 175–177
 323. Hermans, M. M., Kroos, M. A., van Beeumen, J., Oostra, B. A., and Reuser, A. J. (1991) Human lysosomal alpha-glucosidase. Characterization of the catalytic site. *J. Biol. Chem.* **266**, 13507–13512
 324. Galjart, N. J., Morreau, H., Willemsen, R., Gillemans, N., Bonten, E. J., and d'Azzo, A. (1991) Human lysosomal protective protein has cathepsin A-like activity distinct from its protective function. *J. Biol. Chem.* **266**, 14754–14762
 325. Mariappan, M., Li, X., Stefanovic, S., Sharma, A., Mateja, A., Keenan, R. J., et al. (2010) A ribosome-associating factor chaperones tail-anchored membrane proteins. *Nature.* **466**, 1120–1124
 326. Oddo, M., Calandra, T., Bucala, R., and Meylan, P. R. (2005) Macrophage migration inhibitory factor reduces the growth of virulent *Mycobacterium tuberculosis* in human macrophages. *Infect Immun.* **73**, 3783–3786
 327. Ramasamy, V., Ramakrishnan, B., Boeggeman, E., Ratner, D. M., Seeberger, P. H., and Qasba, P. K. (2005) Oligosaccharide preferences of betal, 4-galactosyltransferase-I: crystal structures of Met340His mutant of human betal, 4-galactosyltransferase-I with a pentasaccharide and trisaccharides of the N-glycan moiety. *J. Mol. Biol.* **353**, 53–67
 328. Sayed, M., Pelech, S., Wong, C., Marotta, A., and Salh, B. (2001) Protein kinase CK2 is involved in G2 arrest and apoptosis following spindle damage in epithelial cells. *Oncogene.* **20**, 6994–7005
 329. Kofler, N., Corti, F., Rivera-Molina, F., Deng, Y., Toomre, D., and Simons, M. (2018) The Rab-effector protein RABEP2 regulates endosomal trafficking to mediate vascular endothelial growth factor receptor-2 (VEGFR2)-dependent signaling. *J. Biol. Chem.* **293**, 4805–4817
 330. Klier, H. J., von Figura, K., and Pohlmann, R. (1991) Isolation and analysis of the human 46-kDa mannose 6-phosphate receptor gene. *Eur. J. Biochem.* **197**, 23–28
 331. Mohsen, A. W., and Vockley, J. (1995) Identification of the active site catalytic residue in human isovaleryl-CoA dehydrogenase. *Biochemistry.* **34**, 10146–10152
 332. Zhu, G., Herlyn, M., and Yang, X. (2021) TRIM15 and CYLD regulate ERK activation via lysine-63-linked polyubiquitination. *Nat. Cell Biol.* **23**, 978–991
 333. Cunningham, O., Gore, M. G., and Mantle, T. J. (2000) Initial-rate kinetics of the flavin reductase reaction catalysed by human biliverdin-IXbeta reductase (BVR-B). *Biochem. J.* **345**, 393–399
 334. Braun, E., Hotter, D., Koepke, L., Zech, F., Groß, R., Sparrer, K. M. J., et al. (2019) Guanylate-binding proteins 2 and 5 exert broad antiviral activity by inhibiting furin-mediated processing of viral envelope proteins. *Cell Rep.* **27**, 2092–2104.e10
 335. Stride, B. D., Grant, C. E., Loe, D. W., Hipfner, D. R., Cole, S. P., and Deeley, R. G. (1997) Pharmacological characterization of the murine and human orthologs of multidrug-resistance protein in transfected human embryonic kidney cells. *Mol. Pharmacol.* **52**, 344–353
 336. Veltel, S., Kravchenko, A., Ismail, S., and Wittinghofer, A. (2008) Specificity of Arl2/Arl3 signaling is mediated by a ternary Arl3-effector-GAP complex. *FEBS Lett.* **582**, 2501–2507
 337. Rishavy, M. A., Hallgren, K. W., Yakubenko, A. V., Shtofman, R. L., Runge, K. W., and Berkner, K. L. (2006) Brønsted analysis reveals Lys218 as the carboxylase active site base that deprotonates vitamin K hydroquinone to initiate vitamin K-dependent protein carboxylation. *Biochemistry.* **45**, 13239–13248
 338. Nakatsumi, H., and Yonehara, S. (2010) Identification of functional regions defining different activity in caspase-3 and caspase-7 within cells. *J. Biol. Chem.* **285**, 25418–25425
 339. Raingeaud, J., Whitmarsh, A. J., Barrett, T., Dérjard, B., and Davis, R. J. (1996) MKK3- and MKK6-regulated gene expression is mediated by the p38 mitogen-activated protein kinase signal transduction pathway. *Mol. Cell. Biol.* **16**, 1247–1255
 340. Dumaz, N., Milne, D. M., and Meek, D. W. (1999) Protein kinase CK1 is a p53-threonine 18 kinase which requires prior phosphorylation of serine 15. *FEBS Lett.* **463**, 312–316
 341. Beurel, E., Grieco, S. F., and Jope, R. S. (2015) Glycogen synthase kinase-3 (GSK3): regulation, actions, and diseases. *Pharmacol. Ther.* **148**, 114–131
 342. Shiekhattar, R., Mermelstein, F., Fisher, R. P., Drapkin, R., Dynlacht, B., Wessling, H. C., et al. (1995) Cdk-activating kinase complex is a component of human transcription factor TFIID. *Nature.* **374**, 283–287
 343. Lambrecht, J. A., Flynn, J. M., and Downs, D. M. (2012) Conserved YjgF protein family deaminates reactive enamine/imine intermediates of pyridoxal 5'-phosphate (PLP)-dependent enzyme reactions. *J. Biol. Chem.* **287**, 3454–3461
 344. Savino, T. M., Bastos, R., Jansen, E., and Hernandez-Verdun, D. (1999) The nucleolar antigen Nop52, the human homologue of the yeast ribosomal RNA processing RRP1, is recruited at late stages of nucleologenesis. *J. Cell Sci.* **112**, 1889–1900
 345. Kelkar, A., and Dobberstein, B. (2009) Sec61beta, a subunit of the Sec61 protein translocation channel at the endoplasmic reticulum, is involved in the transport of Gurken to the plasma membrane. *BMC Cell Biol.* **10**, 11

346. Mukhopadhyay, S., and Linstedt, A. D. (2011) Identification of a gain-of-function mutation in a Golgi P-type ATPase that enhances Mn²⁺ efflux and protects against toxicity. *Proc. Natl. Acad. Sci. U. S. A.* **108**, 858–863
347. Grossmann, N., Vakkasoglu, A. S., Hulpke, S., Abele, R., Gaudet, R., and Tampé, R. (2014) Mechanistic determinants of the directionality and energetics of active export by a heterodimeric ABC transporter. *Nat. Commun.* **5**, 5419
348. Taieb, D., Roignot, J., André, F., Garcia, S., Masson, B., Pierres, A., *et al.* (2008) ArgBP2-dependent signaling regulates pancreatic cell migration, adhesion, and tumorigenicity. *Cancer Res.* **68**, 4588–4596
349. Boyle, L., Rao, L., Kaur, S., Fan, X., Mebane, C., Hamm, L., *et al.* (2021) Genotype and defects in microtubule-based motility correlate with clinical severity in. *HGG Adv.* **2**, 100026